

Computational Study on the Unimolecular Decomposition of JP-8 Jet Fuel Surrogates III: Butylbenzene Isomers (*n*-, *s*-, and *t*-C₁₄H₁₀)

Daniel Belisario-Lara and Alexander M. Mebel*[✉]

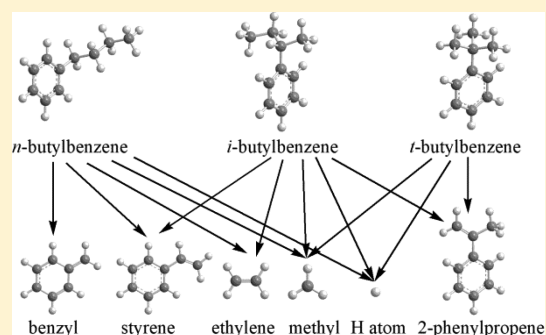
Department of Chemistry and Biochemistry, Florida International University, Miami, Florida 33199, United States

Ralf I. Kaiser*

Department of Chemistry, University of Hawaii at Manoa, Honolulu, Hawaii 96822, United States

ABSTRACT: Ab initio G3(CCSD,MP2)//B3LYP/6-311G(d,p) calculations of potential energy surfaces have been carried out to unravel the mechanism of the initial stages of pyrolysis of three C₁₀H₁₄ isomers: *n*-, *s*-, and *t*-butylbenzenes. The computed energy and molecular parameters have been utilized in RRKM-master equation calculations to predict temperature- and pressure-dependent rate constants and product branching ratios for the primary unimolecular decomposition of these molecules and for the secondary decomposition of their radical fragments. The results showed that the primary dissociation of *n*-butylbenzene produces mostly benzyl (C₇H₇) + propyl (C₃H₇) and 1-phenyl-2-ethyl (C₆H₅C₂H₄) + ethyl (C₂H₅), with their relative yields strongly dependent on temperature and pressure, together with a minor amount of 1-phenyl-prop-3-yl (C₉H₁₁) + methyl (CH₃).

Secondary decomposition reactions that are anticipated to occur on a nanosecond scale under typical combustion conditions split propyl (C₃H₇) into ethylene (C₂H₄) + methyl (CH₃), ethyl (C₂H₅) into ethylene (C₂H₄) + hydrogen (H), 1-phenyl-2-ethyl (C₆H₅C₂H₄) into mostly styrene (C₈H₈) + hydrogen (H) and to a lesser extent phenyl (C₆H₅) + ethylene (C₂H₄), and 1-phenyl-prop-3-yl (C₉H₁₁) into predominantly benzyl (C₇H₇) + ethylene (C₂H₄). The primary decomposition of *s*-butylbenzene is predicted to produce 1-phenyl-1-ethyl (C₆H₅CHCH₃) + ethyl (C₂H₅) and a minor amount of 1-phenyl-prop-1-yl (C₉H₁₁) + methyl (CH₃), and then 1-phenyl-1-ethyl (C₆H₅CHCH₃) and 1-phenyl-prop-1-yl (C₉H₁₁) rapidly dissociate to styrene (C₈H₈) + hydrogen (H) and styrene (C₈H₈) + methyl (CH₃), respectively. *t*-Butylbenzene decomposes nearly exclusively to 2-phenyl-prop-2-yl (C₉H₁₁) + methyl (CH₃), and further, 2-phenyl-prop-2-yl (C₉H₁₁) rapidly eliminates a hydrogen atom to form 2-phenylpropene (C₉H₁₀). If hydrogen atoms or other reactive radicals are available to make a direct hydrogen-atom abstraction from butylbenzenes possible, the C₁₀H₁₃ radicals (1-phenyl-but-1-yl, 2-phenyl-but-2-yl, and *t*-phenyl-isobutyl) can be formed as the primary products from *n*-, *s*-, and *t*-butylbenzene, respectively. The secondary decomposition of 1-phenyl-but-1-yl leads to styrene (C₈H₈) + ethyl (C₂H₅), whereas 2-phenyl-but-2-yl and *t*-phenyl-isobutyl dissociate to 2-phenylpropene (C₉H₁₀) + methyl (CH₃). Thus, the three butylbenzene isomers produce distinct but overlapping nascent pyrolysis fragments, which likely affect the successive oxidation mechanism and combustion kinetics of these JP-8 fuel components. Temperature- and pressure-dependent rate constants generated for the initial stages of pyrolysis of butylbenzenes are recommended for kinetic modeling.



1. INTRODUCTION

Kerosene-based jet fuel JP-8 commonly used in airplanes consists of four main groups of hydrocarbons, which are aliphatic “paraffins” (33–61% *n*-alkanes and isoalkanes; 1–5% olefins), monocyclic “paraffins” (10–20%), alkyl-substituted benzenes (12–22%) including butylbenzenes, and polycyclic aromatic hydrocarbons (PAHs) (10–20%), as well as some additives at the subpercent level including fuel system icing inhibitors, corrosion inhibitors, and static dissipaters.^{1–11} The underlying elementary chemical steps involved in the oxidation of hydrocarbon fuels such as kerosenes are still not completely understood because the current chemical models are unable to account for the complexity of real systems either in the form of multifaceted mixtures of chemicals (as in JP-8) or in the

complexity of the molecular structure of the hydrocarbon itself (as in the synthetic JP-10 fuel). Considering this molecular complexity, Troe¹² and others^{13–16} concluded that this understanding has to commence with the knowledge of the elementary reaction mechanisms of the decomposition of the fuel component itself along with the oxidation of the fragments formed in these processes both experimentally and computationally on the most elementary level. Such understanding can be achieved by using experiments and theory to decouple the pyrolysis of the fuel from the oxidation of relatively small

Received: February 22, 2018

Revised: March 29, 2018

Published: April 2, 2018

individual hydrocarbon fragments and their radicals formed as a result of the pyrolysis. On the basis of sophisticated chemical models, Wang et al.^{17–19} provided compelling evidence that the pyrolysis of hydrocarbon fuels such as JP-8 and JP-10 requires a few tens of microseconds, such as around 20 μ s for the decomposition of dodecane. Since the oxidation of the hydrocarbon fragments occurs on a time scale of typically a few 100 μ s and the ignition engages at normally close to 1000 μ s, the pyrolysis stage can be decoupled from the oxidation chemistry of the hydrocarbon fragments and their radicals. It is therefore critical to determine which particular fragments and in what proportions they are formed at the pyrolysis stage from various significant fuel components.

The development of reliable chemical kinetic models requires accurate input parameters and an intimate understanding of the very first processes, which initiate bond rupture processes in JP-8 components, provide a pool of radicals, and control the autoignition under realistic, combustion-relevant physical conditions.^{10,16,20–22} The unimolecular decomposition, or pyrolysis, of these components leads to smaller hydrocarbon molecules and reactive transient species, among them being aliphatic radicals, resonantly stabilized free radicals, and aromatic radicals, which initiate and drive the complex chemistry in the combustion of JP-8-based jet fuel. Thus, the initial decomposition chemistry delivers the building blocks for the oxidation of JP-8-based jet fuel. In our recent works, we began systematic experimental and theoretical studies on the initial (nascent) products of the pyrolysis of the JP-8 fuel components and probed the pyrolysis of prototype JP-8 aliphatic ingredients *n*-decane C₁₀H₂₂²³ and *n*-dodecane C₁₂H₂₆.²⁴ The pyrolysis was explored in a high-temperature chemical reactor, allowing us to probe the decomposition of a hydrocarbon molecule under combustion-like temperatures of up to 1600 K.²⁵ The nascent product distribution was probed on line and in situ in a supersonic molecular beam utilizing soft photoionization with single-photon vacuum ultraviolet (VUV) photons followed by a mass spectroscopic analysis of the ions in a reflectron time-of-flight mass spectrometer (Re-TOF), which allowed us to detect not only stable fragments but also radicals and thermally labile closed-shell species^{25–34} which usually remain undetected if other experimental techniques are employed. The residence time in the reactor was limited to a few tens of microseconds, and hence we probed the nascent reaction products excluding successive higher-order reactions of the initially formed fragments, which may lead to molecular mass growth processes. The molecular beam experiments were combined with electronic structure and theoretical kinetics calculations, and this synergistic approach elucidated the nature of the products, their branching ratios, and the reaction mechanisms involved in the decomposition of *n*-decane and *n*-dodecane over a broad range of combustion-relevant temperatures and pressures. The theoretical calculations allowed us to account for all pyrolysis products observed experimentally and showed that, under the conditions in the chemical reactor, the primary and fast secondary decomposition reactions (mostly involving C–C and C–H bond β -scissions in the primary radical fragments) need to be considered to explain the nascent product distribution.

The present theoretical work continues this systematic investigation and addresses the prototype representatives of the second largest group of JP-8 components, that is, alkyl-substituted benzenes, in particular, three different isomers of butylbenzene, C₁₀H₁₄: normal (*n*-butylbenzene), 1-*sec* (*s*-

butylbenzene), and *tert* (*t*-butylbenzene). Among the available experimental studies of the decomposition mechanism of these molecules, Yahagi explored the pyrolysis of *t*-butylbenzene in the presence of hydrogen gas at temperatures of up to 923 K. He was able to detect only closed-shell reaction products including benzene, toluene, methane, propene, propane, ethylene, and ethane and inferred a free-radical chain mechanism.³⁵ Early pyrolysis experiments on *n*-butylbenzene followed by the chromatographic detection of aromatic hydrocarbons also proposed radical-initiated chain reactions.³⁶ The involvement of radical transient species likewise gained support from Leigh et al.'s study in which the authors explored the pyrolysis of *n*-butylbenzene and detected ethylene, proposing a radical chain mechanism initiated by the dissociation of *n*-butylbenzene into benzyl and propyl radicals, C₆H₅CH₂CH₂CH₂CH₃ \rightarrow C₆H₅CH₂ + CH₂CH₂CH₃, followed by the decomposition of propyl radicals to ethylene and the methyl radical, CH₃CH₂CH₂ \rightarrow CH₃ + C₂H₄.³⁷ Furthermore, Tsang³⁸ studied the pyrolysis of *t*-butylbenzene, suggesting the existence of C₄H₉ and C₆H₅ transient radicals. Troe and co-workers exploited flash photolysis followed by UV–vis spectroscopy to elucidate the formation of the methyl radical plus the 2-phenyl-prop-2-yl radical in the thermally activated decomposition of *t*-butylbenzene at temperatures ranging from 885 to 1700 K.³⁹ The effect of the molecular structure of the butyl chain (*n*- versus *t*-) in the pyrolysis of butylbenzenes was also investigated by Ma et al.⁴⁰ and Peng et al.,⁴¹ proposing the initial formation of phenyl (C₆H₅) plus *t*-butyl (*t*-C₄H₉) and benzyl (C₆H₅CH₂) and propyl radicals (C₃H₇), respectively. Peng et al. also probed, off line and ex situ, the formation of higher-molecular-weight products such as naphthalene, biphenyl, methylbiphenyl, fluorene, and phenylnaphthalene. While all of these studies provided important data for the development of kinetic models for butylbenzene pyrolysis,⁴² the observed products included not only the nascent but also the higher-order products. Most recently, Zhang et al.⁴³ investigated the pyrolysis of *n*-butylbenzene in a flow reactor with the comprehensive detection of both reactive and stable products using synchrotron vacuum UV photoionization mass spectrometry. They evaluated the mole fractions for a variety of the observed products vs the temperature at different pressures of 30–760 Torr and developed a kinetic model of *n*-butylbenzene pyrolysis using their new data to validate the model. The authors concluded that the benzylic C–C bond dissociation producing benzyl + propyl is the key decomposition reaction.

While kinetic models for the pyrolysis of butylbenzenes have been developed, most of the rate constants utilized in these models, especially those for the initial decomposition steps, are not physics-based; i.e., they are not taken either from experimental kinetics measurements for elementary chemical reactions or from theoretical kinetics calculations based on ab initio potential energy surfaces (PES). These rate constants are either approximately evaluated from analogous reactions, estimated from empirical rate rules, or simply estimated and adjusted to achieve the best fit of the measured concentration profiles for the various species produced in pyrolysis. Theoretically, to our best knowledge, the reaction mechanism, rate constants, and product-branching ratios for the unimolecular decomposition of butylbenzene isomers have never been studied. In fact, high-level reliable theoretical data on the structure and energetics of these molecules computed by ab initio or density functional methods are sparse owing to a relatively large molecular size. Most of the theoretical works

found in the literature address the relative stability of different conformers. Several combined theoretical/experimental studies devoted to the conformational stability, molecular shape, rotational constants, and ionization energies of *n*- and *t*-butylbenzenes have been reported.^{44–48} In terms of thermochemical properties, density functional calculations have been performed to evaluate the enthalpy of formation and C–C bond dissociation energies for *t*-butylbenzene along with *n*-decane and *n*-dodecane.⁴⁹ Theoretical studies of the reaction mechanism and kinetics have been limited to a study of cyclization pathways for the butylbenzene radical⁵⁰ employing rather low-level DFT calculations. The goal of the present work is to bridge the existing knowledge gap: to unravel the pyrolysis mechanism of butylbenzenes based on accurate and reliable calculated PESs, to generate physics-based rate constants for the critical reaction steps, which can be utilized in improved kinetic models, to predict the most important nascent pyrolysis products, and to compare them with the available experimental data.

2. COMPUTATIONAL DETAILS

The geometries of the *n*-, *s*-, and *t*- isomers of butylbenzene C₁₀H₁₄, their primary and secondary decomposition products, and the transition states for the secondary decomposition reactions on the C₁₀H₁₃ PES via C–C and C–H bond β -scissions have been optimized using the density functional B3LYP method^{51,52} with the 6-311G(d,p) basis set. Vibrational frequencies of all stationary structures have been computed at the same B3LYP/6-311G(d,p) level of theory. Relative energies have been refined by single-point calculations using B3LYP/6-311G(d,p) optimized geometries at the G3(CCSD,MP2) level of theory,^{53–55} which included B3LYP/6-311G(d,p) zero-point vibrational energy corrections (ZPE) and empirical higher-level corrections (HLC).⁵⁴ According to the equations for HLC,⁵⁴ which differ for molecules and atoms, the inclusion of the HLC increases the calculated strengths of C–H bonds by 7 kJ mol⁻¹ but is insignificant for C–C bond cleavages and is zero by definition for C–C bond β -scissions in radicals. The G3(CCSD,MP2)//B3LYP theoretical scheme normally provides the energy parameters with “chemical accuracy” within 3–6 kJ mol⁻¹ for hydrocarbons in terms of average absolute deviations.⁵⁴ For secondary reactions on the C₉H₁₁ PES, we used the molecular parameters and energies calculated earlier at a similar G3(CCSD,MP2)//B3LYP level of theory in relation to the C₆H₅ + C₃H₆ reaction.⁵⁶ One additional pathway was calculated and included here, the decomposition of 1-phenylprop-3-yl radical to benzyl + C₂H₄, which was not considered in the previous work. For the decomposition of various primary C₈H₉ products, we employed higher-level calculations where the geometries of various species were optimized and vibrational frequencies were calculated using the double hybrid density functional B2PLYPD3 method^{57–59} with Dunning’s cc-pVDZ basis set,⁶⁰ and single-point energies were refined utilizing the explicitly correlated coupled clusters CCSD(T)-F12 approach^{61,62} with the cc-pVTZ-f12 basis set. All of the ab initio calculations were performed using the Gaussian 09⁶³ and MOLPRO 2010⁶⁴ program packages.

Rate constants for various primary and secondary reactions involved in the pyrolysis of the butylbenzene isomers have been computed using the Rice–Ramsperger–Kassel–Marcus master equation (RRKM-ME) approach by solving the one-dimensional master equation⁶⁵ employing the MESS package.⁶⁶ Rate constants $k(T)$ for individual reaction steps were calculated

within RRKM (unimolecular reactions) or transition-state theory (TST, bimolecular reactions) generally utilizing the rigid rotor harmonic oscillator (RRHO) model for the calculations of partition functions for molecular complexes and transition states. Hindered rotor treatment for low-frequency torsional modes was applied only to smaller C₉H₁₁ and C₈H₉ systems for which such “soft” normal modes were visually examined and those representing internal rotations were considered to be hindered rotors in partition function calculations. One-, two-, and even three- (for some C₉H₁₁ structures⁶⁷) dimensional torsional potentials were calculated by scanning the PES at the B3LYP/6-311G(d,p) level of theory. However, for butylbenzenes themselves and C₁₀H₁₃ radicals, hindered rotor treatment is rather complicated because they possess up to four hindered rotors corresponding to four different single bonds, and these rotors could be strongly coupled. For simplicity, all these convoluted rotations were treated as harmonic oscillators. In our earlier work,²³ we compared the results of the RRHO treatment with and without the inclusion of hindered rotors for smaller C₃H₇ and C₄H₉ radicals and found maximal deviations in rate constants of 41% at 1000 K and 25% at 1600 K. Therefore, the initial C–C and C–H bond cleavages in butylbenzenes were treated within RRHO, keeping in mind the above-mentioned error bars in rate constants. It should be noted that absolute errors in the partition function caused by the treatment of torsional modes as harmonic oscillators in a molecule with multiple coupled torsional modes could be much larger, one to two orders of magnitude according to Truhlar and co-workers,⁶⁸ but the smaller errors in the rate constants observed in our calculations likely resulted from the cancellation of larger errors in the partition functions of transition states (in the numerator) and reactants (in the denominator) on the basis of the fact that in the transition states and reactants most of the torsional modes (besides one or two) are similar. For a system with a small number of torsional modes (ethanol), Truhlar and co-workers found the effect of more accurate internal-coordinate multi-structural treatment to be within a factor of 1.8–3.4 as compared to that of the use of harmonic oscillators; these values should be considered to be an upper limit for error bars of our pure RRHO calculations. The errors in ratios of rate constants are expected to be smaller than the errors in their absolute values due to the cancellations of similar inaccuracies, and hence we anticipate that relative product yields are predicted by our calculations with higher accuracy.

Collisional energy transfer rates in the master equation were expressed using the “exponential down” model,⁶⁹ with the temperature dependence of range parameter α for the deactivating wing of the energy transfer function expressed as $\alpha(T) = \alpha_{300}(T/300 \text{ K})^n$, with $n = 0.86$ and $\alpha_{300} = 228 \text{ cm}^{-1}$ obtained earlier from classical trajectory calculations as “universal” parameters for hydrocarbons in the nitrogen bath gas.⁷⁰ For RRKM-ME calculations on the C₁₀H₁₄ and C₁₀H₁₃ PESs, we used the Lennard–Jones parameters (ϵ/cm^{-1} , $\sigma/\text{\AA}$) = (237, 5.02) for the *n*-decane/nitrogen system derived by Jasper et al.⁷⁰ based on the fit of results using the “one-dimensional optimization” method.⁷¹ For the calculations on the C₉H₁₁ surface, we used the collision parameters employed earlier in the study of the C₆H₅ + C₃H₆ system; in fact, we used the MESS input file for this system given in ref 67 and augmented it with the transition state and bimolecular products on the additional pathways leading from benzyl + C₂H₄. Finally, RRKM-ME calculations on the C₈H₉ surface utilized the

collision parameters $n = 0.61$ and $\alpha_{300} = 375 \text{ cm}^{-1}$ and $(\epsilon/\text{cm}^{-1}, \sigma/\text{\AA}) = (317, 4.46)$ derived earlier for the $\text{C}_6\text{H}_5 + \text{C}_2\text{H}_2$ system.⁷²

The MESS package uses the eigenvalue approach for solving a master equation, and for a well-defined description of a phenomenological rate constant to exist, chemical time scales (CSEs) must be well separated from vibrational–rotational time scales (IEREs).⁷³ When CSEs and IEREs overlap, the determination of phenomenological rate constants is compromised and no predictions can be made for isomers that rapidly equilibrate (merge) with other, more stable isomers or decomposition products. Merging with decomposition products often occurs in the systems considered here at high temperatures for closed-shell molecules and even at moderate temperatures for radicals. In such cases, we used the language throughout the article stating that a certain species does not survive above a certain temperature at a given pressure, meaning that this species rapidly equilibrates with its decomposition products under these conditions but the phenomenological rate constant for the decomposition process is not well-defined.

For barrierless reactions, such as the C–C and C–H single-bond cleavages in the original butylbenzene molecules, we used phase space theory.⁷⁴ The reverse rate constants for the recombination of two hydrocarbon radicals or of a radical and H were fitted using potential parameters (prefactor and power exponent) to reproduce the most accurate available rate constants for the prototype $\text{CH}_3 + \text{C}_2\text{H}_5$, $\text{C}_2\text{H}_5 + \text{C}_2\text{H}_5$, $\text{CH}_3 + i\text{-C}_3\text{H}_7$, $\text{C}_2\text{H}_5 + i\text{-C}_3\text{H}_7$, $\text{CH}_3 + t\text{-C}_4\text{H}_9$, $\text{C}_2\text{H}_5 + t\text{-C}_4\text{H}_9$, benzyl $\text{C}_7\text{H}_7 + \text{H}$, $\text{C}_2\text{H}_5 + \text{H}$, and $t\text{-C}_4\text{H}_9 + \text{H}$ calculated earlier by Klippenstein and co-workers^{75–77} using variable reaction coordinated transition state theory (VRC-TST). For each particular case of a C–C or C–H bond cleavage in butylbenzenes, the most appropriate prototype reaction was selected based on chemical similarity (see Table 1), and the fits to the VRC-TST rate constants were attained within an accuracy of 1–2% in the entire 500–2500 K temperature range. Then, the fitted parameters were used in phase-space theory calculations of rate constants for the decomposition reactions with the MESS package, which also gave results on pressure dependence. The accuracy of the rate constants of the barrierless single-bond cleavages also relies upon the accuracy of equilibrium constants, which in turn is determined by the accuracy of the calculated reaction energy (3–6 kJ mol⁻¹ for the G3(CCSD,MP2)//B3LYP method) and the accuracy of the molecular parameters including rotational constants and vibrational frequencies, which is generally considered to be adequate for the B3LYP method.

3. RESULTS AND DISCUSSION

3.1. *n*-Butylbenzene. We first consider the primary decomposition pathways of *n*-butylbenzene illustrated in Figure 1. There are three different C–C bond cleavages, which are favorable energetically. Those lead to the benzyl $\text{C}_7\text{H}_7 + \text{propyl C}_3\text{H}_7$ products with an endothermicity of 341 kJ mol⁻¹, 1-phenyl-prop-3-yl $\text{C}_9\text{H}_{11} + \text{methyl CH}_3$ (369 kJ mol⁻¹), and $\text{C}_6\text{H}_5\text{C}_2\text{H}_4 + \text{ethyl C}_2\text{H}_5$ (375 kJ mol⁻¹). The cleavage of the C–C bond adjacent to the benzene ring and forming phenyl $\text{C}_6\text{H}_5 + 1\text{-butyl C}_4\text{H}_9$ is much less favorable (448 kJ mol⁻¹). Among C–H bond cleavages, the most favorable one occurs from the α carbon in the side chain producing 1-phenyl-but-1-yl with an energy loss of 369 kJ mol⁻¹. The other H losses from sp^3 carbon atoms require higher energies of 411, 408, and 420

Table 1. Prototype Reactions of the Recombination of Two Hydrocarbon Radicals or of a Radical and an H Used for the Fitting of Potential Parameters in Phase-Space Calculations of Rate Constants of Barrierless Reactions

reactant	products	prototype reaction	reference
<i>n</i> -butylbenzene	C_9H_{11} (1-phenyl-prop-3-yl) + CH_3	$\text{C}_2\text{H}_5 + \text{CH}_3$	75
<i>n</i> -butylbenzene	$\text{C}_8\text{H}_9 + \text{C}_2\text{H}_5$	$\text{C}_2\text{H}_5 + \text{C}_2\text{H}_5$	75
<i>n</i> -butylbenzene	$\text{C}_7\text{H}_7 + \text{C}_3\text{H}_7$	$\text{C}_2\text{H}_5 + \text{C}_2\text{H}_5$	75
<i>n</i> -butylbenzene	$\text{C}_6\text{H}_5 + \text{C}_4\text{H}_9$ (1-yl)	$\text{C}_2\text{H}_5 + \text{C}_2\text{H}_5$	75
<i>n</i> -butylbenzene	$\text{C}_{10}\text{H}_{13}$ (1-yl) + H	$\text{C}_7\text{H}_7 + \text{H}$	77
<i>n</i> -butylbenzene	$\text{C}_{10}\text{H}_{13}$ (2-yl) + H	$\text{C}_2\text{H}_5 + \text{H}$	76
<i>n</i> -butylbenzene	$\text{C}_{10}\text{H}_{13}$ (3-yl) + H	$\text{C}_2\text{H}_5 + \text{H}$	76
<i>n</i> -butylbenzene	$\text{C}_{10}\text{H}_{13}$ (4-yl) + H	$\text{C}_2\text{H}_5 + \text{H}$	76
<i>s</i> -butylbenzene	C_9H_{11} (2-phenyl-prop-1-yl) + CH_3	$\text{C}_2\text{H}_5 + \text{CH}_3$	75
<i>s</i> -butylbenzene	$\text{C}_8\text{H}_9 + \text{C}_2\text{H}_5$	$i\text{-C}_3\text{H}_7 + \text{C}_2\text{H}_5$	75
<i>s</i> -butylbenzene	C_9H_{11} (1-phenyl-prop-1-yl) + CH_3	$i\text{-C}_3\text{H}_7 + \text{CH}_3$	75
<i>s</i> -butylbenzene	$\text{C}_6\text{H}_5 + \text{C}_4\text{H}_9$ (2-yl)	$i\text{-C}_3\text{H}_7 + \text{C}_2\text{H}_5$	75
<i>s</i> -butylbenzene	$\text{C}_{10}\text{H}_{13}$ (1-yl) + H	$\text{C}_2\text{H}_5 + \text{H}$	76
<i>s</i> -butylbenzene	$\text{C}_{10}\text{H}_{13}$ (2-yl) + H	$i\text{-C}_3\text{H}_7 + \text{H}$	75
<i>s</i> -butylbenzene	$\text{C}_{10}\text{H}_{13}$ (3-yl) + H	$i\text{-C}_3\text{H}_7 + \text{H}$	75
<i>s</i> -butylbenzene	$\text{C}_{10}\text{H}_{13}$ (4-yl) + H	$\text{C}_2\text{H}_5 + \text{H}$	76
<i>t</i> -butylbenzene	C_9H_{11} (2-phenyl-prop-2-yl) + CH_3	$t\text{-C}_4\text{H}_9 + \text{CH}_3$	75
<i>t</i> -butylbenzene	$\text{C}_6\text{H}_5 + t\text{-C}_4\text{H}_9$	$t\text{-C}_4\text{H}_9 + \text{C}_2\text{H}_5$	75
<i>t</i> -butylbenzene	$\text{C}_{10}\text{H}_{13} + \text{H}$	$\text{C}_2\text{H}_5 + \text{H}$	76

kJ mol⁻¹ and forming the corresponding 2-yl, 3-yl, and 4-yl 1-phenyl-butyl radicals, respectively. We do not consider here the ruptures of C–H bonds on the sp^2 carbons of the aromatic ring, which are unlikely to compete because their bond energies are typically much higher, e.g., 466 kJ mol⁻¹ for benzene.⁷⁸ Figure 2a illustrates the total rate constant for the unimolecular decomposition of *n*-butylbenzene calculated at the high-pressure limit (HP) and finite pressures of 30 Torr and 1, 10, and 100 atm. The calculated rate constants were fitted by modified Arrhenius expressions, which are assembled in Table 2. One can observe a falloff behavior of the rate constants and that at finite pressures *n*-butylbenzene can survive dissociation only up to a certain temperature; 1650, 1800, 2000, and 2250 K at 30 Torr, 1, 10, and 100 atm, respectively. At higher temperatures, the lifetime of *n*- $\text{C}_{10}\text{H}_{14}$ becomes shorter than the time interval between collision, and the RRKM-ME rate constant is no longer well-defined. In practice, this means that beyond these temperature thresholds, *n*-butylbenzene would instantly equilibrate with its bimolecular decomposition products. The falloff behavior is manifested, for example, by the fact that at 1500 K the rate constants calculated at 30 Torr and 1, 10, and 100 atm are factors of 9.2, 2.3, 1.3, and 1.1 lower than the HP values, and the deviation from the HP limit further increases with temperature. According to the calculated branching ratios for the dissociation of *n*-butylbenzene (see Figure 2b and Table 3), the $\text{C}_7\text{H}_7 + \text{C}_3\text{H}_7$ products are preferable at lower temperatures, but as temperature increases, the relative yield of $\text{C}_6\text{H}_5\text{C}_2\text{H}_4 + \text{C}_2\text{H}_5$ grows faster and becomes nearly equal to or higher than that of $\text{C}_7\text{H}_7 + \text{C}_3\text{H}_7$. The formation of $\text{C}_6\text{H}_5\text{C}_2\text{H}_4 + \text{C}_2\text{H}_5$ is also favored by pressure; at 2500 K and 100 atm, the calculated $\text{C}_6\text{H}_5\text{C}_2\text{H}_4 + \text{C}_2\text{H}_5/\text{C}_7\text{H}_7 + \text{C}_3\text{H}_7$ branching ratio reaches 1.5. The $\text{C}_9\text{H}_{11} + \text{CH}_3$ products are predicted to be minor, with the maximal branching ratio of ~6% at the highest temperature and pressure

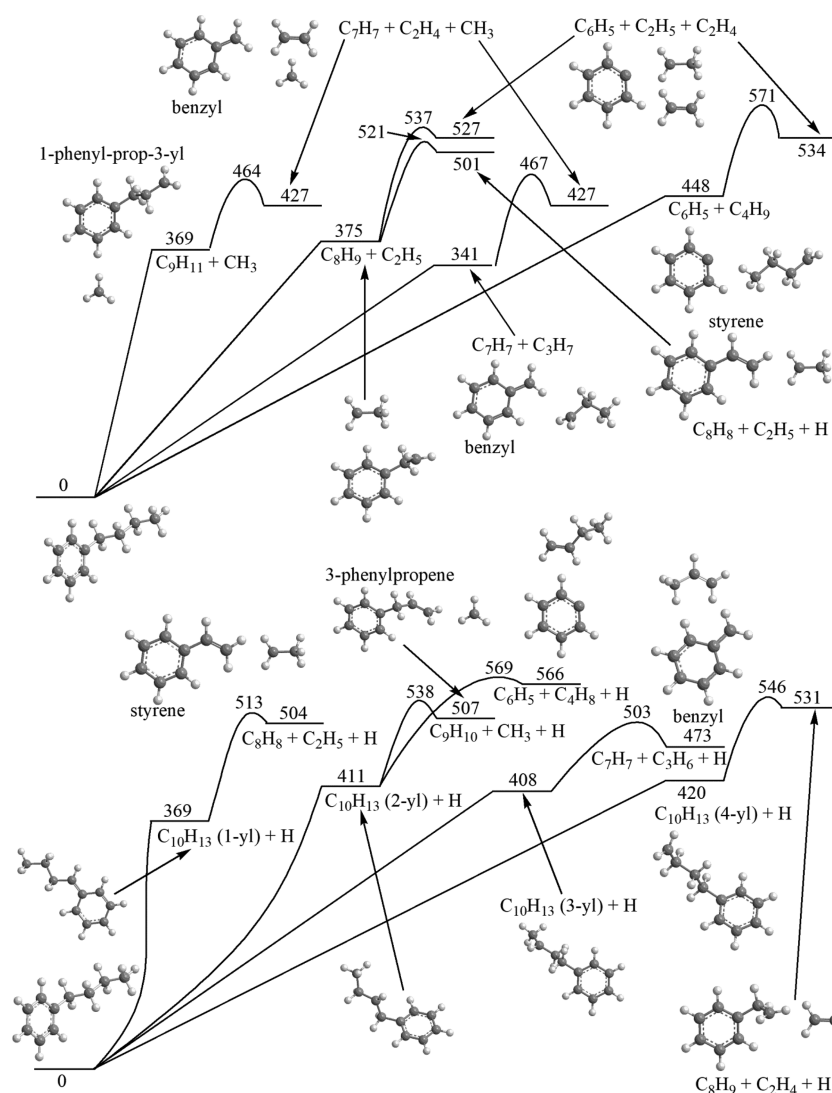


Figure 1. Potential energy diagram for the primary and most favorable secondary decomposition channels of *n*-butylbenzene. All relative energies with respect to the parent molecule are given in kJ mol⁻¹.

considered. The calculated branching ratios of all other products do not exceed 0.3%. In summary, the primary decomposition of *n*-butylbenzene is predicted to predominantly produce the benzyl radical + C₃H₇ and C₈H₉ (C₆H₅C₂H₄) + C₂H₅. Under the typical combustion conditions of 1500 K and 1 atm, the lifetime of *n*-butylbenzene is computed to be as short as 2.9 μs. We discussed in the previous works that C₃H₇ is likely to further decompose to C₂H₄ + CH₃, whereas C₂H₅ dissociates to C₂H₄ + H.^{23,24} The secondary decomposition of the C₈H₉ and C₉H₁₁ isomers will be considered in subsequent sections.

3.2. *s*-Butylbenzene. The unimolecular decomposition pathways of *s*-butylbenzene include C–C and C–H bond cleavages illustrated in Figure 3. The most favorable energy channels of C–C bond cleavages lead to 1-phenyl-prop-1-yl C₉H₁₁ + CH₃ (326 kJ mol⁻¹) and C₆H₅CHCH₃ + C₂H₅ (328 kJ mol⁻¹) followed by 2-phenyl-prop-3-yl C₉H₁₁ + CH₃, which is endothermic by 371 kJ mol⁻¹. The pathway leading to C₆H₅ + 2-butyl C₄H₉ is by far the least preferable, with the reaction energy of 424 kJ mol⁻¹. Among C–H bond cleavages, the channel in which a hydrogen atom is eliminated from the carbon atom linked to the phenyl group has the lowest

endoothermicity of 366 kJ mol⁻¹ and forms a 2-phenyl-but-2-yl radical. The other sp³ C–H bonds are stronger, and their cleavages produce corresponding 1-yl, 3-yl, and 4-yl 2-phenyl-butyl radicals with reaction energies of 419, 408, and 419 kJ mol⁻¹, respectively. As seen in Figure 4a, the total rate constant for the unimolecular decomposition of *s*-butylbenzene behaves in a similar way as that for *n*-butylbenzene. The calculations indicate that *s*-C₁₀H₁₄ can survive up to 1500, 1800, 1800, and 2000 K at pressures of 30 Torr and 1, 10, and 100 atm, respectively, and rapidly equilibrates with its bimolecular products at higher temperatures. The falloff behavior is somewhat more pronounced than for *n*-C₁₀H₁₄; at 1500 K, the finite pressure decomposition rate constants at 30 Torr and 1, 10, and 100 atm are factors of 18.8, 3.4, 1.6, and 1.1 lower than the HP limit value, respectively. *s*-Butylbenzene is anticipated to be less stable than *n*-butylbenzene with respect to pyrolysis, as the lifetime computed at 1500 K and 1 atm is only 0.8 μs. In terms of the calculated branching ratios (Figure 4b and Table 3), C₆H₅CHCH₃ and C₂H₅ are predicted to be the main decomposition products (83–86%) of *s*-C₁₀H₁₄ followed by 1-phenyl-prop-1-yl and CH₃ (14–15%), whereas 2-phenyl-prop-3-yl and CH₃ are minor products with a relative

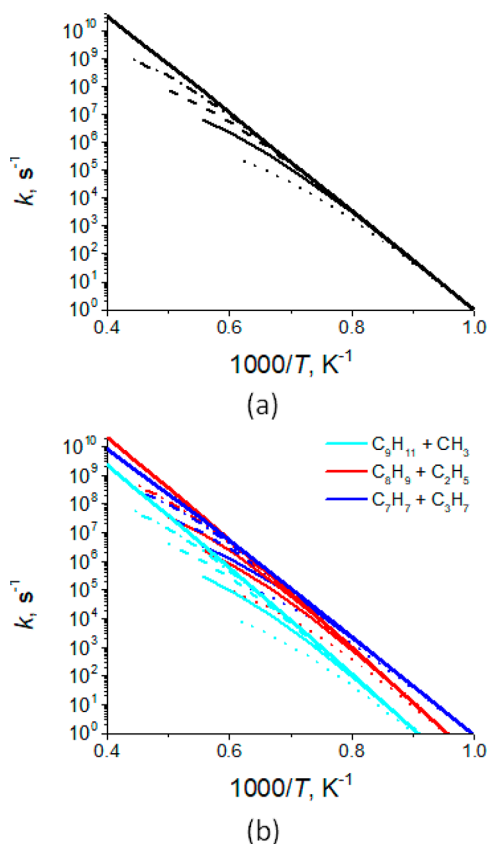


Figure 2. Total (a) and individual channel (b) rate constants for the primary decomposition of *n*-butylbenzene. The dotted, solid, dashed, and dotted–dashed curves show values calculated at pressures of 30 Torr and 1, 10, and 100 atm, respectively. The bold curve in panel (a) shows the HP limit total rate constant.

yield normally below 1% but increasing to 1.6% at 100 atm and 2000 K. The relative yields of all of the other products of C–C and C–H bond cleavages do not exceed 0.1%. The product branching ratios appeared to be nearly insensitive to pressure (Table 3).

3.3. *t*-Butylbenzene. Taking into account a nearly free rotation of the phenyl group around the C–C bond linked to the central C atom, one can consider *t*-butylbenzene to be C_{3v} -symmetric. In addition, each methyl group possesses local C_3 symmetry. As a consequence of such a symmetric structure, only three distinct C–C and C–H bond cleavage channels exist if we exclude unfavorable H eliminations from the aromatic ring (Figure 5). A methyl group loss producing 2-phenyl-prop-2-yl is the least endothermic process (318 kJ mol⁻¹), whereas the other two channels producing $C_6H_5 + t$ -butyl C_4H_9 and *t*-phenyl-isobutyl $C_{10}H_{13} + H$ require much higher energies to occur, 412 and 421 kJ mol⁻¹, respectively. This large difference in the bond strengths is reflected in the fact that 2-phenyl-prop-2-yl and CH_3 are predicted to be nearly exclusive products of the pyrolysis of *t*-butylbenzene with its calculated branching ratio exceeding 99% at all considered temperatures and pressures. Figure 6 illustrates the overall rate constant for the unimolecular decomposition of *t*- $C_{10}H_{14}$, which is nearly identical to the rate constant of the channel producing 2-phenyl-prop-2-yl + CH_3 . Clearly, this rate constant behaves in a similar way to those for *n*- and *s*-butylbenzenes considered above. Because of the weak tertiary/benzylic C–C bond in *t*-butylbenzene, the rate constant is faster than the corresponding

value for *n*-butylbenzene but comparable with that for *s*-butylbenzene. For instance, at 1500 K and 1 atm, the rate constant for the unimolecular decomposition of *t*- $C_{10}H_{14}$ is 1.29×10^6 s⁻¹ (corresponding to a lifetime of 0.78 μs) compared to 3.39×10^5 s⁻¹ (2.9 μs) and 1.23×10^6 s⁻¹ (0.81 μs) for *n*- and *s*- $C_{10}H_{14}$, respectively. Similar to *s*- $C_{10}H_{14}$, at the pressures of 30 Torr and 1, 10, and 100 atm, *t*-butylbenzene can survive at up to 1500, 1800, 1800, and 2000 K, respectively, and at higher temperatures, it should be considered to be equilibrated with the 2-phenyl-prop-2-yl and CH_3 products. The falloff behavior of the *t*-butylbenzene decomposition rate constant is also similar to that of *s*- $C_{10}H_{14}$, as the finite pressure values at 1500 K and 30 Torr and 1, 10, and 100 atm are factors of 17.4, 3.2, 1.5, and 1.1 lower than the HP limit rate constant, respectively.

Having established the predominant primary pyrolytic products of the three different butylbenzene isomers ($C_7H_7 + C_3H_7$ and $C_6H_5C_2H_4 + C_2H_5$ for *n*- $C_{10}H_{14}$, $C_6H_5CHCH_3 + C_2H_5$ and 1-phenyl-prop-1-yl $C_9H_{11} + CH_3$ for *s*- $C_{10}H_{14}$, and 2-phenyl-prop-2-yl $C_9H_{11} + CH_3$ for *t*- $C_{10}H_{14}$), we now move to consider the secondary decomposition channels not studied earlier in detail in the literature and, in particular, discuss the unimolecular decomposition of C_8H_9 and C_9H_{11} isomers and the related reactions on the corresponding PESs. In addition, we consider the decomposition of the most favorable $C_{10}H_{13}$ products, which, though unlikely to be formed directly via unimolecular dissociation of butylbenzenes, could be produced by H-atom abstraction reactions by other radicals, such as by H atoms.

3.4. Reactions on the C_8H_9 PES. The most favorable decomposition pathways of $C_6H_5C_2H_4$ (W1) and $C_6H_5CHCH_3$ (W2), which are also related to the reaction of phenyl radical C_6H_5 with ethylene C_2H_4 , are illustrated in Figure 7. The $C_6H_5C_2H_4$ isomer can dissociate through a C–H β-scission reaction forming styrene via a barrier of 146 kJ mol⁻¹ and a C–C β-scission process via a barrier of 162 kJ mol⁻¹, with endothermicities of 126 and 152 kJ mol⁻¹, respectively. Alternatively, W1 can isomerize to W2 or W3 via 1,2-H or 1,4-H shifts, overcoming lower barriers of 138 and 123 kJ mol⁻¹, respectively. Four-membered ring closure in W1 leading to bicyclic structure W4 is also possible via a 133 kJ mol⁻¹ barrier. Since W3 cannot directly decompose to any energetically favorable product, it is most likely to isomerize back to W1. On the other hand, W4 can dissociate to 1,2-dihydrobenzocyclobutene (1,2-DHB) and H, which lie 24 and 50 kJ mol⁻¹ above the $C_6H_5 + C_2H_4$ and styrene + H bimolecular products, respectively. The most stable $C_6H_5CHCH_3$ isomer (W2) dissociates to styrene and H to overcome a 187 kJ mol⁻¹ barrier or rearranges to W1 via a 191 kJ mol⁻¹ barrier, but the isomerization of W2 to W3 via a 1,3-H shift is not competitive because of a much higher barrier of 269 kJ mol⁻¹.

It should be noted that the relative energies of various species calculated here at the CCSD(T)-F12/cc-pVTZ-f12//B2PLYPD3/cc-pVDZ level of theory agree within 5 kJ mol⁻¹ with the results obtained by Tokmakov and Lin at the G2M level,⁷⁹ with the average absolute deviation between the two methods being 1.8 kJ mol⁻¹. The G2M approach is similar to that of G3(CCSD,MP2) employed for the $C_{10}H_{14}$ systems in the present study, and the two methods normally provide comparable accuracies. Also, our recent calculations on the C_9H_{10} PES in relation to the $C_6H_5 + C_3H_5$ reaction (to be published elsewhere) gave the average absolute deviation

Table 2. Rate Constants Calculated in the Present Work in the Form $AT^\alpha \exp(-E_a/RT)$ and the Temperature Range Where They Are Applicable^a

reaction	A	α	E_a	T range, K
<i>n</i> -Butylbenzene → Products				
k_{30} Torr	0.2819×10^{137}	-34.472	0.15131×10^6	1000–1650
k_1 atm	0.1514×10^{105}	-24.839	0.13586×10^6	1000–1800
k_{10} atm	0.15814×10^{83}	-18.397	0.12380×10^6	1000–2000
k_{100} atm	0.55489×10^{64}	-13.048	0.11285×10^6	1000–2250
<i>n</i> -Butylbenzene → C ₈ H ₉ ^b + C ₂ H ₃				
k_{30} Torr	0.4541×10^{120}	-29.747	0.14297×10^6	800–1650
k_1 atm	0.56452×10^{89}	-20.480	0.12839×10^6	800–1800
k_{10} atm	0.71658×10^{95}	-21.854	0.13808×10^6	1000–2000
k_{100} atm	0.32344×10^{75}	-15.953	0.12606×10^6	1000–2250
<i>n</i> -Butylbenzene → C ₇ H ₇ + C ₃ H ₇				
k_{30} Torr	0.2936×10^{136}	-34.289	0.14966×10^6	1000–1650
k_1 atm	0.5569×10^{104}	-24.857	0.13397×10^6	1000–1800
k_{10} atm	0.81242×10^{83}	-18.768	0.12229×10^6	1000–2000
k_{100} atm	0.55318×10^{66}	-13.803	0.11194×10^6	1000–2250
<i>t</i> -Butylbenzene → C ₉ H ₁₁ ^c + CH ₃				
k_{30} Torr	0.3349×10^{130}	-32.822	0.13649×10^6	900–1500
k_1 atm	0.2732×10^{103}	-24.610	0.12490×10^6	900–1800
k_{10} atm	0.12936×10^{74}	-16.037	0.10842×10^6	900–1800
k_{100} atm	0.40728×10^{63}	-12.875	0.10409×10^6	1000–2000
<i>s</i> -Butylbenzene → Products				
k_{30} Torr	0.1022×10^{133}	-33.478	0.13945×10^6	900–1500
k_1 atm	0.4768×10^{106}	-25.477	0.12841×10^6	900–1800
k_{10} atm	0.22139×10^{77}	-16.894	0.11201×10^6	900–1800
k_{100} atm	0.16494×10^{67}	-13.826	0.10813×10^6	1000–2000
<i>s</i> -Butylbenzene → C ₈ H ₉ ^d + C ₂ H ₃				
k_{30} Torr	0.7368×10^{132}	-33.459	0.13935×10^6	900–1500
k_1 atm	0.2680×10^{106}	-25.429	0.12821×10^6	900–1800
k_{10} atm	0.20675×10^{77}	-16.911	0.11195×10^6	900–1800
k_{100} atm	0.22675×10^{67}	-13.891	0.10817×10^6	1000–2000
<i>s</i> -Butylbenzene → C ₉ H ₁₁ ^e + CH ₃				
k_{30} Torr	0.5915×10^{132}	-33.641	0.14007×10^6	900–1500
k_1 atm	0.2386×10^{106}	-25.614	0.12907×10^6	900–1800
k_{10} atm	0.85572×10^{76}	-16.996	0.11265×10^6	900–1800
k_{100} atm	0.71654×10^{66}	-13.939	0.10886×10^6	1000–2000
C ₆ H ₅ + C ₂ H ₄ → Products				
k_{30} Torr	9.4464×10^5	1.8693	2239.3	300–2500
k_1 atm	2.0100×10^6	1.778	2397.9	300–2500
k_{10} atm	2.3850×10^6	1.7637	2465.7	300–2500
k_{100} atm	1.2054×10^6	1.8615	2394.3	300–2500
C ₆ H ₅ + C ₂ H ₄ → C ₆ H ₅ C ₂ H ₄ ^f				
k_{30} Torr	8.2987×10^{66}	-16.65	29108	300–1250
	6.0680×10^{27}	-5.4215	7398.1	
k_1 atm	1.1171×10^{54}	-12.347	27727	300–1500
	1.0473×10^{19}	-2.448	5490.5	
k_{10} atm	1.1757×10^{45}	-9.4512	26260	300–1800
	2.3841×10^{15}	-1.2167	4684.2	
k_{100} atm	1.3233×10^{39}	-7.5071	26252	300–2250
	1.1015×10^{13}	-0.42344	4186.9	
C ₆ H ₅ + C ₂ H ₄ → C ₆ H ₅ CHCH ₃				
k_{30} Torr ^f	3.4678×10^{98}	-25.624	52593	700–1375
	1.3945×10^{93}	-12.561	278220	
k_1 atm	0.13775×10^{72}	-16.892	48548	800–1650
k_{10} atm	0.14061×10^{82}	-19.331	63732	900–1800
k_{100} atm	0.32995×10^{73}	-16.446	69092	1125–2000
C ₆ H ₅ + C ₂ H ₄ → Styrene + H				
k_{30} Torr	9881.3	-4.0434	22708	700–2500
k_1 atm	0.24473×10^{13}	-6.1864	34763	700–2500
k_{10} atm	14153.	-3.7364	34237	700–2500
k_{100} atm	0.77121×10^{-15}	1.7171	25424	700–2500

Table 2. continued

reaction	A	α	E_a	T range, K
$C_6H_5C_2H_4 \rightarrow C_6H_5CHCH_3$				
k_{30} Torr	0.13729×10^{78}	-19.670	61528	700–1250
k_1 atm	0.42526×10^{54}	-12.317	53277.	700–1500
k_{10} atm	0.23604×10^{41}	-8.2442	48021.	700–1800
k_{100} atm	0.57326×10^{26}	-3.8783	40985.	700–2000
$C_6H_5C_2H_4 \rightarrow C_6H_5 + C_2H_4$				
k_{30} Torr	0.13570×10^{69}	-16.765	63658	700–1250
k_1 atm	0.62212×10^{47}	-10.064	56335.	700–1500
k_{10} atm	0.12289×10^{35}	-6.1854	51030.	700–1800
k_{100} atm ^f	0.64577×10^{97}	-23.062	0.11331×10^6	800–2250
	0.57481×10^{47}	-9.9048	58034.	
$C_6H_5C_2H_4 \rightarrow$ Styrene + H				
k_{30} Torr	0.28862×10^{57}	-9.9048	56563.	700–1250
k_1 atm	0.21594×10^{35}	-13.172	47730	700–1500
k_{10} atm	0.16083×10^{25}	-6.3698	43274	700–1800
k_{100} atm	0.29775×10^{18}	-1.2907	40057	700–2250
$C_6H_5CHCH_3 \rightarrow C_6H_5C_2H_4$				
k_{30} Torr	0.87116×10^{79}	-19.756	74462	700–1250
k_1 atm	0.37632×10^{56}	-12.448	66269.	700–1500
k_{10} atm	0.81224×10^{51}	-10.800	67018.	800–1800
k_{100} atm	0.45661×10^{34}	-5.6827	58279.	800–2000
$C_6H_5CHCH_3 \rightarrow C_6H_5 + C_2H_4$				
k_{30} Torr	0.71658×10^{81}	-19.817	88471	800–1375
k_1 atm	0.64321×10^{74}	-17.086	95109	800–1650
k_{10} atm	0.62466×10^{98}	-23.549	0.11889×10^6	900–1800
k_{100} atm	0.90966×10^{78}	-17.558	0.11501×10^6	1000–2000
$C_6H_5CHCH_3 \rightarrow$ Styrene + H				
k_{30} Torr	0.39723×10^{67}	-15.788	70609.	700–1350
k_1 atm	0.54825×10^{47}	-9.6498	62984.	700–1650
k_{10} atm	0.17259×10^{38}	-6.7433	59099	700–1800
k_{100} atm	0.10842×10^{27}	-3.4126	53546	700–2000
1-Phenyl-prop-3-yl $\rightarrow C_7H_7 + C_2H_4$				
k_{30} Torr	0.15181×10^{42}	-9.1509	33677.	500–1000
k_1 atm	0.11961×10^{25}	-3.6943	28267.	500–1250
k_{10} atm	0.28783×10^{17}	-1.3103	25564.	500–1500
k_{100} atm	0.62196×10^{12}	0.12868	23764.	500–1800
1-Phenyl-prop-1-yl \rightarrow Styrene + CH_3				
k_{30} Torr	0.75140×10^{74}	-18.351	60229.	600–1125
k_1 atm	0.43845×10^{49}	-10.417	51483.	600–1250
k_{10} atm	0.16947×10^{38}	-6.8643	47292.	600–1500
k_{100} atm	0.14615×10^{26}	-3.2006	42095.	600–1650
2-Phenyl-prop-3-yl \rightarrow 1-Phenyl-prop-2-yl				
k_{30} Torr	0.12762×10^{44}	-10.176	26387	500–800
k_1 atm	0.38095×10^{22}	-3.3033	19250.	500–1000
k_{10} atm	0.21159×10^{19}	-2.2313	18455.	500–1375
k_{100} atm	0.29014×10^{15}	-1.0251	17071.	500–1650
2-Phenyl-prop-3-yl \rightarrow Styrene + CH_3				
k_{30} Torr	0.31994×10^{15}	-0.81166	28179.	500–800
k_1 atm	0.25419×10^{26}	-3.9024	33731.	500–1000
k_{10} atm	0.12159×10^{23}	-2.7569	33242.	500–1375
k_{100} atm	0.11140×10^{17}	-0.87002	31080.	500–1650
2-Phenyl-prop-3-yl \rightarrow 3-Phenylpropene + H				
k_{30} Torr	0.13864×10^{36}	-6.6219	43792.	500–800
k_1 atm	0.14349×10^{32}	-5.0212	46967.	500–1000
k_{10} atm	0.33583×10^{60}	-13.223	65893.	700–1375
k_{100} atm	0.29057×10^{52}	-10.680	67198.	800–1650
1-Phenyl-prop-2-yl \rightarrow 2-Phenyl-prop-3-yl				
k_{30} Torr	0.16346×10^{36}	-7.7720	25155.	500–800
k_1 atm	0.23712×10^{20}	-2.6140	20735.	500–1000
k_{10} atm	0.34657×10^{17}	-1.6706	20110.	500–1375
k_{100} atm	0.67814×10^{13}	-0.51112	18791.	500–1650

Table 2. continued

reaction	A	α	E_a	T range, K
1-Phenyl-prop-2-yl \rightarrow C ₆ H ₅ + C ₃ H ₆				
k_{30} Torr	0.23039×10^{85}	-21.670	67957.	700–1125
k_1 atm	0.64665×10^{60}	-13.875	59910.	700–1250
k_{10} atm	0.31641×10^{49}	-10.287	56360.	700–1500
k_{100} atm	0.88533×10^{51}	-10.680	61805	900–1800
1-Phenyl-prop-2-yl \rightarrow Styrene + CH ₃				
k_{30} Torr	0.52521×10^{80}	-20.237	61759.	700–1125
k_1 atm	0.15314×10^{53}	-11.447	55588.	700–1250
k_{10} atm ^f	0.15110×10^{59}	-13.055	63048.	700–1500
	0.13760×10^{46}	4.7394	0.35964×10^6	
k_{100} atm ^f	0.31534×10^{51}	-10.663	64204.	800–1800
	0.36860×10^{16}	14.560	0.44487×10^6	
1-Phenyl-prop-2-yl \rightarrow 3-Phenylpropene + H				
k_{30} Torr	0.17142×10^{81}	-20.308	64300.	700–1125
k_1 atm	0.84166×10^{58}	-13.226	56888.	700–1250
k_{10} atm	0.35020×10^{49}	-10.188	54496.	700–1500
k_{100} atm ^f	0.44975×10^{127}	-31.498	0.12347×10^6	800–1800
	0.10754×10^{67}	-15.311	64197.	
2-Phenyl-prop-2-yl \rightarrow 3-Phenylpropene + H				
k_{30} Torr	0.82275×10^{73}	-17.737	68952	700–1250
k_1 atm	0.44801×10^{49}	-10.263	59400	700–1500
k_{10} atm	0.78328×10^{37}	-6.6856	54392	700–1800
k_{100} atm	0.15315×10^{26}	-3.2056	48571	700–2000
C ₇ H ₇ + C ₂ H ₄ \rightarrow Products				
k_{30} Torr	0.42341×10^{-40}	14.665	-24338.	800–2500
k_1 atm ^f	0.11413×10^{99}	-25.294	57307.	800–2500
	0.15521×10^{48}	-8.8630	64946.	
k_{10} atm ^f	0.35603×10^{48}	-10.228	32510.	800–2500
	0.11245×10^{156}	-37.117	0.20054×10^6	
k_{100} atm	0.32724×10^{17}	-1.1416	15300.	800–2500
C ₇ H ₇ + C ₂ H ₄ \rightarrow 1-Phenyl-prop-3-yl				
k_{30} Torr	0.23483×10^{68}	-16.985	33840.	800–1000
k_1 atm	0.16908×10^{46}	-9.8538	27855.	800–1250
k_{10} atm	0.60656×10^{27}	-4.2276	20084.	800–1500
k_{100} atm	0.52053×10^{14}	-0.32926	13689.	800–1800
C ₇ H ₇ + C ₂ H ₄ \rightarrow 3-Phenylpropene + H				
k_{30} Torr	0.13513×10^{11}	1.0092	24577.	1000–2500
k_1 atm	0.68819×10^{20}	-1.6066	34206.	1000–2500
k_{10} atm	0.36348×10^{34}	-5.2361	50066.	1000–2500
k_{100} atm	0.32342×10^{36}	-5.5410	59858.	1250–2500
C ₇ H ₇ + C ₂ H ₄ \rightarrow Indane + H				
k_{30} Torr	1.07908×10^{07}	0.97799	8157.	1125–2500
k_1 atm	6.50858×10^{28}	-4.8767	30219.	1125–2500
k_{10} atm	1.85809×10^{44}	-8.9065	50055.	1125–2500
k_{100} atm	9.83814×10^{29}	-4.7424	47447.	1125–2500
1-Phenyl-but-1-yl \rightarrow Styrene + C ₂ H ₅				
k_{30} Torr	0.11163×10^{81}	-20.325	60678.	600–1000
k_1 atm	0.13319×10^{57}	-12.713	53067.	600–1250
k_{10} atm	0.81005×10^{39}	-7.3967	46363.	600–1375
k_{100} atm	0.44185×10^{29}	-4.2512	42200.	800–1650
2-Phenyl-but-2-yl \rightarrow 2-Phenylpropene + CH ₃				
k_{30} Torr	0.11181×10^{82}	-20.500	63498.	600–1000
k_1 atm	0.15319×10^{59}	-13.217	56310.	600–1250
k_{10} atm	0.52362×10^{41}	-7.8218	49528.	600–1375
k_{100} atm	0.37016×10^{37}	-6.4139	49329.	700–1650
<i>t</i> -Phenyl-isobutyl \rightarrow 2-Phenylpropene + CH ₃				
k_{30} Torr	0.10652×10^{77}	-19.449	52578.	600–900
k_1 atm	0.15257×10^{53}	-11.783	45522.	600–1125
k_{10} atm	0.10899×10^{36}	-6.4538	39110.	600–1250
k_{100} atm	0.97064×10^{25}	-3.3583	35144.	600–1500

Table 2. continued

reaction	A	α	E_a	T range, K
<i>t</i> -Phenyl-isobutyl \rightarrow Phenyl + Isobutene				
$k_{0.03}$ atm	0.57120×10^{90}	-23.742	63227.	600–900
k_1 atm	0.27287×10^{74}	-18.087	61565.	700–1125
k_{10} atm	0.14084×10^{54}	-11.708	54635.	700–1250
k_{100} atm	0.22147×10^{36}	-6.2632	47250.	700–1500

^aUnits are s⁻¹ (unimolecular reactions), cm³ mol⁻¹ s⁻¹ (bimolecular reactions), and cal/mol for E_a . ^bC₆H₅C₂H₄. ^c2-Phenyl-prop-2-yl. ^dC₆H₅CHCH₃. ^e1-Phenyl-prop-1-yl. ^fIf two lines of the parameters are given for a particular pressure, then an accurate fit (within 10%) of the calculated rate constants can be achieved only by a sum of two modified Arrhenius expressions.

Table 3. Calculated Product Branching Ratios in the Primary Decomposition of *n*- and *s*-Butylbenzenes

T, K	<i>p</i>											
	30 Torr			1 atm			10 atm			100 atm		
	<i>n</i> -Butylbenzene											
	C ₉ H ₁₁ ^a + CH ₃	C ₈ H ₉ ^b + C ₂ H ₅	C ₇ H ₇ + C ₃ H ₇	C ₉ H ₁₁ ^a + CH ₃	C ₈ H ₉ ^b + C ₂ H ₅	C ₇ H ₇ + C ₃ H ₇	C ₉ H ₁₁ ^a + CH ₃	C ₈ H ₉ ^b + C ₂ H ₅	C ₇ H ₇ + C ₃ H ₇	C ₉ H ₁₁ ^a + CH ₃	C ₈ H ₉ ^b + C ₂ H ₅	C ₇ H ₇ + C ₃ H ₇
1000	1.70%	13.59%	84.70%	1.79%	14.40%	83.79%	1.79%	14.49%	83.70%	1.80%	14.50%	83.69%
1125	2.27%	18.64%	79.07%	2.54%	21.15%	76.27%	2.59%	21.61%	75.76%	2.60%	21.69%	75.67%
1250	2.70%	22.52%	74.75%	3.20%	27.20%	69.54%	3.35%	28.60%	67.98%	3.39%	28.97%	67.57%
1375	3.01%	25.36%	71.58%	3.70%	31.90%	64.31%	3.99%	34.61%	61.28%	4.09%	35.64%	60.13%
1500	3.24%	27.50%	69.21%	4.07%	35.33%	60.49%	4.47%	39.28%	56.08%	4.68%	41.28%	53.82%
1650	3.45%	29.49%	66.99%	4.37%	38.29%	57.19%	4.89%	43.30%	51.58%	5.21%	46.50%	47.96%
1800				4.60%	40.47%	54.76%	5.17%	46.11%	48.43%	5.59%	50.21%	43.76%
2000							5.44%	48.75%	45.45%	5.92%	53.55%	39.94%
2250										6.19%	56.26%	36.80%
	<i>s</i> -Butylbenzene											
	C ₉ H ₁₁ ^c + CH ₃	C ₈ H ₉ ^d + C ₂ H ₅	C ₉ H ₁₁ ^e + CH ₃	C ₉ H ₁₁ ^c + CH ₃	C ₈ H ₉ ^d + C ₂ H ₅	C ₉ H ₁₁ ^e + CH ₃	C ₉ H ₁₁ ^c + CH ₃	C ₈ H ₉ ^d + C ₂ H ₅	C ₉ H ₁₁ ^e + CH ₃	C ₉ H ₁₁ ^c + CH ₃	C ₈ H ₉ ^d + C ₂ H ₅	C ₉ H ₁₁ ^e + CH ₃
1000	0.09%	86.13%	13.77%	0.12%	86.03%	13.85%	0.12%	86.01%	13.86%	0.12%	86.01%	13.87%
1125	0.14%	85.87%	13.99%	0.21%	85.63%	14.16%	0.23%	85.56%	14.20%	0.24%	85.55%	14.21%
1250	0.18%	85.67%	14.14%	0.31%	85.30%	14.39%	0.38%	85.14%	14.48%	0.40%	85.08%	14.50%
1375	0.22%	85.53%	14.24%	0.40%	85.04%	14.55%	0.53%	84.77%	14.69%	0.61%	84.62%	14.75%
1500	0.25%	85.42%	14.32%	0.48%	84.84%	14.66%	0.68%	84.46%	14.84%	0.83%	84.19%	14.95%
1650				0.57%	84.66%	14.76%	0.83%	84.16%	14.97%	1.10%	83.73%	15.12%
1800				0.64%	84.50%	14.84%	0.97%	83.92%	15.07%	1.34%	83.34%	15.24%
2000										1.62%	82.92%	15.36%

^a1-Phenyl-prop-3-yl. ^bC₆H₅C₂H₄. ^c2-Phenyl-prop-3-yl. ^dC₆H₅CHCH₃. ^e1-Phenyl-prop-1-yl.

between the CCSD(T)-F12/cc-pVTZ-f12 and G3-(CCSD,MP2) energies as 2.3 kJ mol⁻¹, and the maximal deviation was about 6 kJ mol⁻¹. Therefore, one can expect that the CCSD(T)-F12/cc-pVTZ-f12 method should improve the accuracy of the energies as compared to G3(CCSD,MP2) by about 2 kJ mol⁻¹ on average.

Rate constants for the unimolecular decomposition of C₆H₅C₂H₄ and C₆H₅CHCH₃ are illustrated in Figure 8a,b. At low temperatures, W1 would mostly isomerize to W2 and W3, which gets collisionally stabilized, but the reaction is too slow. As temperature increases, the relative yield of the bimolecular products, styrene + H and C₆H₅ + C₂H₄, increases while that of the stabilized intermediates decreases. As seen in Table 4, the branching ratio of styrene and H exceeds that of W1 at temperatures of 1125, 1375, 1650, and 1800 K if the pressure is 30 Torr and 1, 10, and 100 atm, respectively. At these pressures, C₆H₅C₂H₄ is predicted to survive up to 1250, 1500, 1650, and 2250 K, respectively, and at the higher temperatures it would rapidly equilibrate with the bimolecular products, predominantly styrene and H. The relative yield of C₆H₅ + C₂H₄ is generally smaller but grows with temperature up to 20–24%. Similarly, W2 isomerizes to W1 at low temperatures and predominantly dissociates to styrene + H as the

temperature increases. Here, the decomposition channel takes over at a much lower temperature than for W1, 600 K at all considered pressures. W2 is predicted to be more stable than W1 and to survive up to 1375, 1650, 1800, and 2000 K at 30 Torr and 1, 10, and 100 atm, respectively. The predominant dissociation channel of W2 is styrene + H, with C₆H₅ + C₂H₄ contributing less than 10% even at high temperatures. Under the typical combustion conditions of 1500 K and 1 atm, the rate constants for the C₆H₅C₂H₄ \rightarrow styrene + H/C₆H₅ + C₂H₄ routes are 1.30×10^7 and 3.96×10^6 s⁻¹, respectively, corresponding to the overall lifetime of this radical with respect to the decomposition channels of only 58 ns. Under the same conditions, the rate constants for the decomposition of C₆H₅CHCH₃ to styrene + H and C₆H₅ + C₂H₄, respectively, are 7.34×10^6 and 3.03×10^5 s⁻¹, and hence the lifetime of the more stable C₈H₉ isomer, W2, is longer at 131 ns. Clearly, both C₆H₅C₂H₄ and C₆H₅CHCH₃, if formed as primary pyrolysis products of butylbenzenes, would undergo fast secondary dissociation to styrene + H and a minor amount of C₆H₅ + C₂H₄ on a nanosecond scale under typical combustion conditions.

It is also informative to compare the present results for the C₆H₅ + C₂H₄ reaction with the previous experimental and

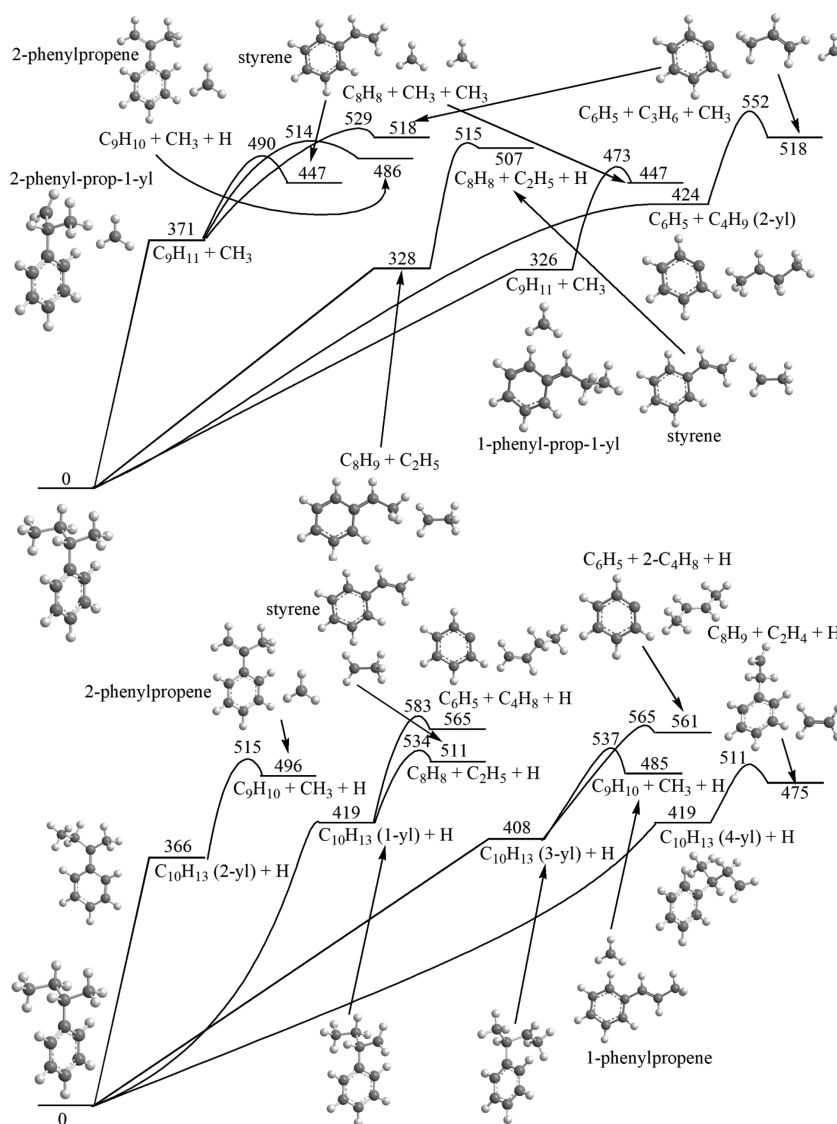


Figure 3. Potential energy diagram for the primary and most favorable secondary decomposition channels of *s*-butylbenzene. All relative energies with respect to the parent molecule are given in kJ mol^{-1} .

theoretical data. Figure 8c compares the overall rate constant computed here with the theoretical prediction of Tokmakov and Lin⁷⁹ based on their G2M PES and the experimental values of Yu and Lin⁸⁰ in the low-temperature range of 300–500 K and of Fahr et al.^{81,82} at higher temperatures of 1000–1400 K. There is a very close match between the two sets of theoretical rate constants, which agree within 32%. In the low-temperature range, the present calculated rate values overestimate the experimental results by Yu and Lin by factors of 1.36–2.36, but the agreement with the high-temperature measurements by Fahr et al. is within 10%. Figure 8c also shows that the total rate constants for the $\text{C}_6\text{H}_5 + \text{C}_2\text{H}_4$ reaction are nearly indistinguishable at the four finite pressures considered here, and their falloff from the HP limit values maximal at 2500 K is only a factor of 1.4. Alternatively, relative product yields in the $\text{C}_6\text{H}_5 + \text{C}_2\text{H}_4$ reaction are sensitive to both temperature and pressure (Figure 8d and Table 4). At low temperatures, the stabilized $\text{C}_6\text{H}_4\text{C}_2\text{H}_4$ intermediate W1 is the main product, but at higher temperatures, the reaction predominantly forms styrene + H. The switch in the preference of these two products occurs around 1000, 1375, 1650, and 2050 K at

pressures of 30 Torr and 1, 10, and 100 atm, respectively, and in the highest temperature intervals considered where W1 is no longer stable, styrene and H become practically the exclusive reaction products.

3.5. Reactions on the C_9H_{11} PES. For a detailed description of the C_9H_{11} surface in relation to the $\text{C}_6\text{H}_5 + \text{C}_3\text{H}_6$ reaction, we direct the reader to our previous work.⁵⁶ Kinetic calculations on this PES were also described earlier,⁶⁷ but they mostly addressed bimolecular product formation in the reaction of phenyl with propene. Here, our interest is the unimolecular decomposition of various C_9H_{11} isomers produced as primary products of pyrolysis of butylbenzenes. We employ the same surface and molecular parameters published earlier while considering these decomposition reactions. However, since the 1-phenyl-prop-3-yl ($\text{C}_6\text{H}_5\text{CH}_2\text{CH}_2\text{CH}_2$) \rightarrow benzyl + C_2H_4 dissociation channel was not considered in the previous studies, it is included here. The present G3(CCSD,MP2)//B3LYP/6-311G(d,p) calculations gave the barrier and endothermicity for this C–C β -scission reaction as 95 and 58 kJ mol^{-1} , respectively. The benzyl + C_2H_4 bimolecular products reside 85 kJ mol^{-1} below

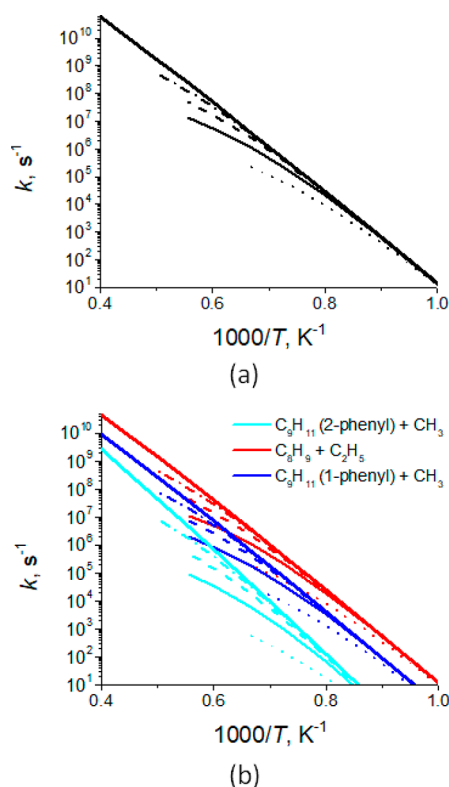


Figure 4. Total (a) and individual channel (b) rate constants for the primary decomposition of *s*-butylbenzene. The dotted, solid, dashed, and dotted–dashed curves show values calculated at pressures of 30 Torr and 1, 10, and 100 atm, respectively. The bold curve in panel (a) shows the HP limit total rate constant.

$C_6H_5 + C_3H_6$ and are also more thermodynamically favorable than styrene + CH_3 , 3-phenylpropene + H, *trans*- and *cis*-1-

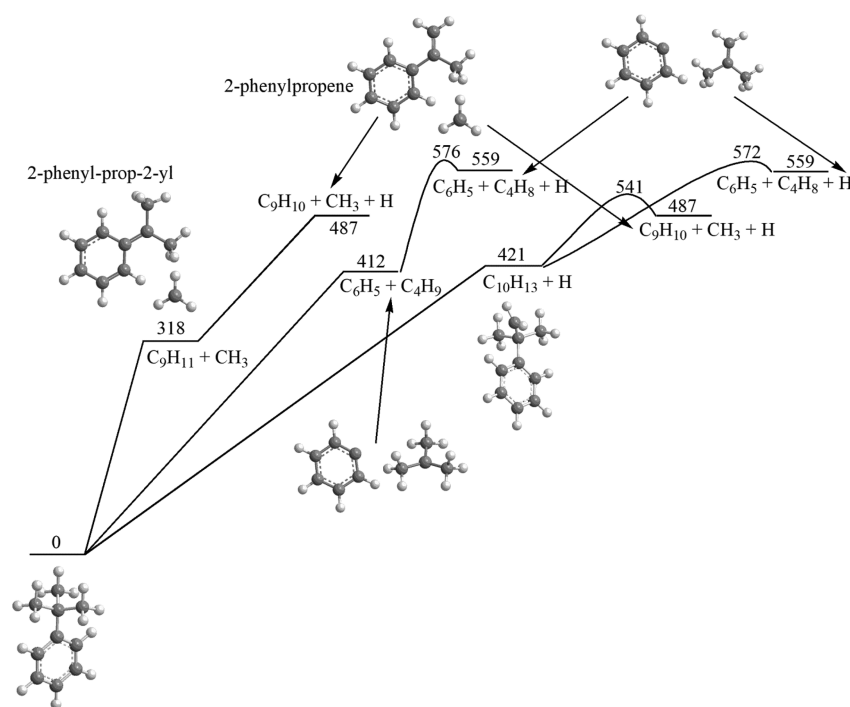


Figure 5. Potential energy diagram for the primary and most favorable secondary decomposition channels of *t*-butylbenzene. All relative energies with respect to the parent molecule are given in kJ mol^{-1} .

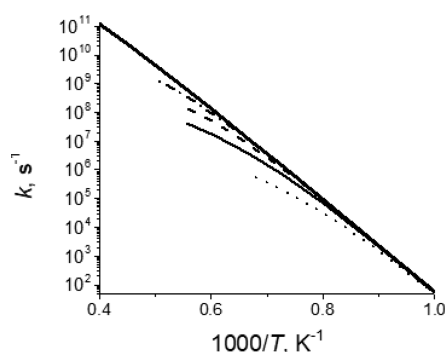


Figure 6. Total rate constant for the primary decomposition of *t*-butylbenzene, which nearly exclusively produces 2-phenyl-prop-2-yl and CH_3 . The dotted, solid, dashed, and dotted–dashed curves show values calculated at pressures of 30 Torr and 1, 10, and 100 atm, respectively. The bold curve shows the HP limit total rate constant.

phenylpropenes + H, and 2-phenylpropene by 15, 71, 52, 60, and 53 kJ mol^{-1} , respectively.

Calculations of the rate constants for the unimolecular dissociation of 1-phenyl-prop-3-yl (Figure 9a), which can be formed in the primary decomposition of *n*-butylbenzene, show that this C_9H_{11} radical predominantly decomposes to benzyl + C_2H_4 , with the yield of the alternative products, indane + H and 3-phenylpropene + H, not exceeding 5 and 14%, respectively (Table 5). 1-Phenyl-prop-3-yl can survive only up to 1000, 1250, 1500, and 1800 K at 30 Torr and 1, 10, and 100 atm, respectively, and its lifetime at 1250 K and 1 atm is evaluated to be 21 ns. Therefore, it can be safely assumed that under typical combustion conditions 1-phenyl-prop-3-yl rapidly dissociates mostly to benzyl and ethylene on a nanosecond scale or faster. The primary pyrolysis of *s*-butylbenzene can produce two C_9H_{11} isomers, 1-phenyl-prop-1-yl and 2-phenyl-prop-3-yl, and their unimolecular decomposition rate constants are shown in

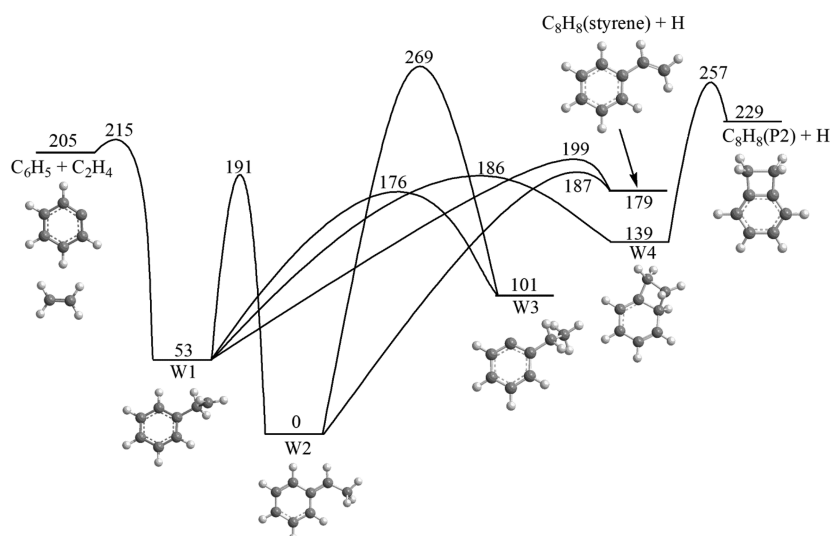


Figure 7. Potential energy diagram for the unimolecular decomposition of the $C_6H_5C_2H_4$ (W1) and $C_6H_5CHCH_3$ (W2) isomers of C_8H_9 , and the $C_6H_5 + C_2H_4$ reaction. All relative energies with respect to $C_6H_5CHCH_3$ are given in kJ mol^{-1} .

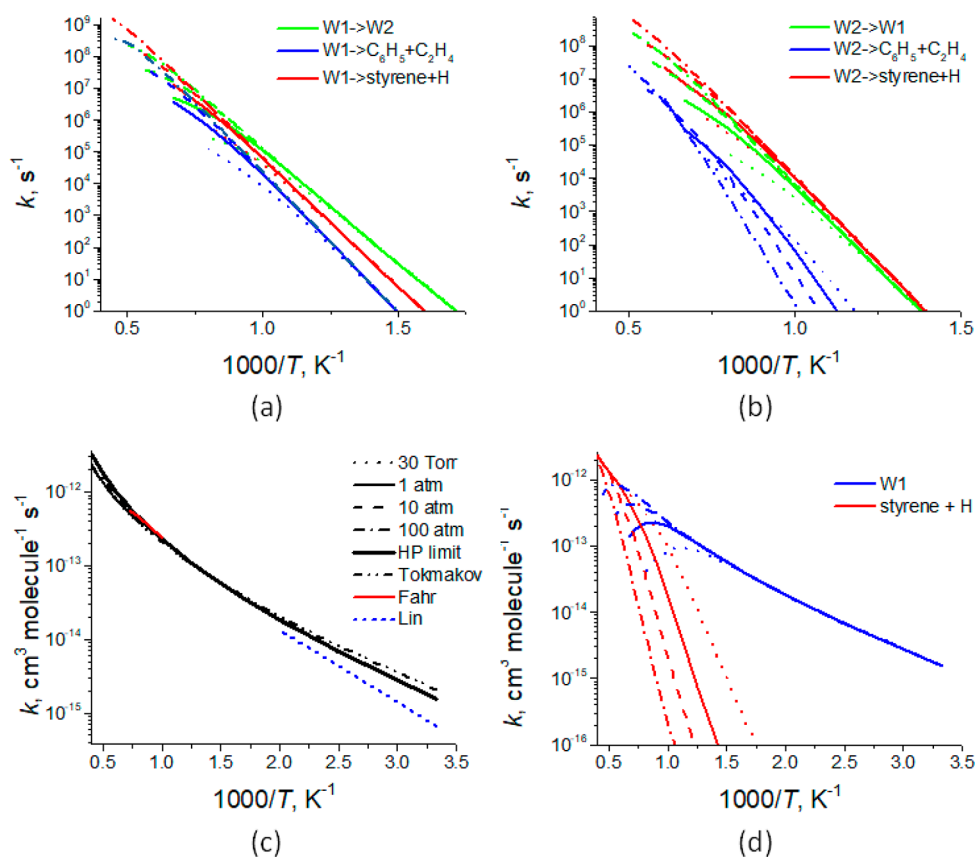


Figure 8. Rate constants for various reactions involving the C_8H_9 PES: (a) the isomerization and unimolecular decomposition of $C_6H_5C_2H_4$; (b) the isomerization and unimolecular decomposition of $C_6H_5CHCH_3$; (c) the total rate constant for the $C_6H_5 + C_2H_4$ reaction in comparison with the literature values from Tokmakov and Lin (ref 79), Yu and Lin (ref 80), and Fahr et al. (refs 81 and 82); and (d) the individual rate constants for the stabilization of $C_6H_5C_2H_4$ (W1) and the formation of styrene and H in the $C_6H_5 + C_2H_4$ reaction. The dotted, solid, dashed, and dotted–dashed curves show values calculated at pressures of 30 Torr and 1, 10, and 100 atm, respectively. The bold curve in panel (c) shows the HP limit total rate constant.

Figure 9b,c. 1-Phenyl-prop-1-yl appears to be slightly more stable than 1-phenyl-prop-3-yl as it can be collisionally stabilized up to 1125, 1250, 1500, and 1650 K at the four pressures considered here, and its lifetime at 1250 K and 1 atm is computed as 43 ns. The predominant decomposition

products of 1-phenyl-prop-1-yl is styrene and CH_3 formed by C–C β -scission, whereas the yield of *trans*-1-phenylpropene and H, while increasing with temperature and pressure, does not exceed 8%. 2-Phenyl-prop-3-yl (denoted as W2 in our previous work on the kinetics of the $C_6H_5 + C_3H_6$ reaction⁶⁷)

Table 4. Calculated Product Branching Ratios of Various Reactions on the C₈H₉ PES

C ₆ H ₅ C ₂ H ₄ (W1) → Products																
<i>p</i>																
T, K	30 Torr				1 atm				10 atm				100 atm			
	W2	W3	C ₆ H ₅ + C ₂ H ₄	styrene + H	W2	W3	C ₆ H ₅ + C ₂ H ₄	styrene + H	W2	W3	C ₆ H ₅ + C ₂ H ₄	styrene + H	W2	W3	C ₆ H ₅ + C ₂ H ₄	styrene + H
600	33.63%	61.46%	0.51%	4.41%	25.39%	70.39%	0.39%	3.31%	24.15%	70.10%	0.37%	3.15%	24.15%	70.10%	0.37%	3.15%
700	51.37%	34.94%	1.98%	11.72%	35.96%	54.66%	1.44%	7.94%	32.06%	57.17%	1.29%	7.06%	32.06%	57.17%	1.29%	7.06%
800	58.32%		4.22%	20.62%	44.64%	37.65%	3.46%	14.25%	37.53%	45.58%	2.93%	11.84%	37.53%	45.58%	2.93%	11.84%
900	60.74%		7.01%	32.24%	49.11%	23.68%	6.13%	21.08%	40.57%	35.98%	5.10%	16.65%	40.57%	35.98%	5.10%	16.65%
1000	50.95%		8.73%	40.32%	48.79%	14.69%	8.82%	27.70%	42.36%	28.72%	7.62%	21.29%	42.36%	28.72%	7.62%	21.29%
1125	38.94%		10.58%	50.48%	47.85%		12.84%	39.32%	42.15%	21.27%	10.63%	25.95%	42.15%	21.27%	10.63%	25.95%
1250	28.62%		12.12%	59.26%	38.38%		14.92%	46.70%	40.76%	15.90%	13.36%	29.99%	40.76%	15.90%	13.36%	29.99%
1375					29.84%		16.63%	53.53%	38.30%	12.12%	15.71%	33.86%	38.30%	12.12%	15.71%	33.86%
1500					22.95%		18.01%	59.04%	34.83%	9.55%	17.69%	37.92%	34.83%	9.55%	17.69%	37.92%
									29.85%		19.64%	42.93%	29.85%		19.64%	42.93%
									26.26%		22.66%	51.04%	26.26%		22.66%	51.04%
									19.94%		24.09%	55.94%	19.94%		24.09%	55.94%
											18.86%	81.10%			18.86%	81.10%

C ₆ H ₅ CHCH ₃ (W2) → Products												
T, K	30 Torr			1 atm			10 atm			100 atm		
	W1	C ₆ H ₅ + C ₂ H ₄	styrene + H	W1	C ₆ H ₅ + C ₂ H ₄	styrene + H	W1	C ₆ H ₅ + C ₂ H ₄	styrene + H	W1	C ₆ H ₅ + C ₂ H ₄	styrene + H
700	41.20%	0.07%	58.70%	41.79%	0.00%	58.19%	41.84%	0.00%	58.16%	41.84%	0.00%	58.16%
800	36.92%	0.30%	62.73%	39.03%	0.03%	60.90%	39.24%	0.00%	60.75%	39.27%	0.00%	60.73%
900	32.38%	0.76%	66.86%	37.05%	0.14%	62.76%	37.78%	0.02%	62.18%	37.89%	0.00%	62.10%
1000	27.55%	1.40%	71.05%	34.86%	0.40%	64.65%	36.75%	0.07%	63.12%	37.13%	0.01%	62.85%
1125	22.52%	2.20%	75.28%	31.46%	1.02%	67.53%	35.37%	0.27%	64.26%	36.58%	0.04%	63.35%
1250	19.30%	2.81%	77.90%	27.68%	1.80%	70.52%	33.38%	0.70%	65.78%	36.09%	0.13%	63.71%
1375		6.54%	93.46%	24.56%	2.52%	72.91%	31.05%	1.31%	67.64%	35.35%	0.34%	64.20%
1500				22.42%	3.07%	74.50%	28.61%	1.96%	69.42%	34.18%	0.68%	64.97%
1650					10.12%	89.88%	26.30%	2.63%	71.07%	32.39%	1.23%	66.16%
1800							24.79%	3.11%	72.10%	30.86%	1.79%	67.35%
2000										29.06%	2.39%	68.55%

C ₆ H ₅ + C ₂ H ₄ → Products												
<i>p</i>												
T, K	30 Torr			1 atm			10 atm			100 atm		
	W1	W2	styrene + H	W1	W2	styrene + H	W1	W2	styrene + H	W1	W2	styrene + H
300	99.99%	0.00%	0.00%	100.00%	0.00%	0.00%	100.00%	0.00%	0.00%	100.00%	0.00%	0.00%
400	99.93%	0.03%	0.01%	100.00%	0.00%	0.00%	100.00%	0.00%	0.00%	100.00%	0.00%	0.00%
500	99.64%	0.24%	0.07%	99.98%	0.01%	0.00%	100.00%	0.00%	0.00%	100.00%	0.00%	0.00%
600	98.12%	1.24%	0.57%	99.89%	0.06%	0.02%	99.99%	0.01%	0.00%	100.00%	0.00%	0.00%
700	92.69%	4.17%	3.05%	99.51%	0.28%	0.14%	99.94%	0.03%	0.01%	99.99%	0.00%	0.00%
800	80.21%	8.86%	10.78%	98.18%	1.02%	0.68%	99.76%	0.12%	0.07%	99.97%	0.01%	0.01%
900	61.35%	12.49%	26.16%	94.49%	2.77%	2.55%	99.22%	0.40%	0.28%	99.91%	0.04%	0.03%
1000	40.94%	12.32%	46.74%	86.76%	5.52%	7.41%	97.77%	1.09%	0.95%	99.73%	0.13%	0.10%
1125	21.14%	8.18%	70.67%	71.43%	8.68%	19.88%	93.43%	2.82%	3.41%	99.09%	0.42%	0.38%
1250	9.71%	4.15%	86.13%	52.41%	9.20%	38.39%	84.98%	5.14%	9.31%	97.50%	1.09%	1.19%
1375		3.07%	96.62%	34.80%	7.37%	57.82%	73.40%	6.84%	19.75%	94.26%	2.22%	3.13%
1500			99.97%	21.28%	4.98%	73.72%	59.13%	7.13%	33.73%	88.84%	3.58%	6.97%

Table 4. continued

T, K	$C_6H_5 + C_2H_4 \rightarrow$ Products											
	p											
	30 Torr			1 atm			10 atm			100 atm		
	W1	W2	styrene + H	W1	W2	styrene + H	W1	W2	styrene + H	W1	W2	styrene + H
1650			99.96%		5.99%	92.66%	42.16%	6.05%	51.76%	79.42%	4.89%	14.70%
1800			99.94%			99.94%	27.82%	4.42%	67.71%	68.94%	5.43%	25.61%
2000			99.91%			99.91%			99.91%	52.26%	5.03%	42.66%
2250			99.87%			99.87%			99.87%	30.92%		68.97%
2500			99.82%			99.82%			99.82%			99.82%

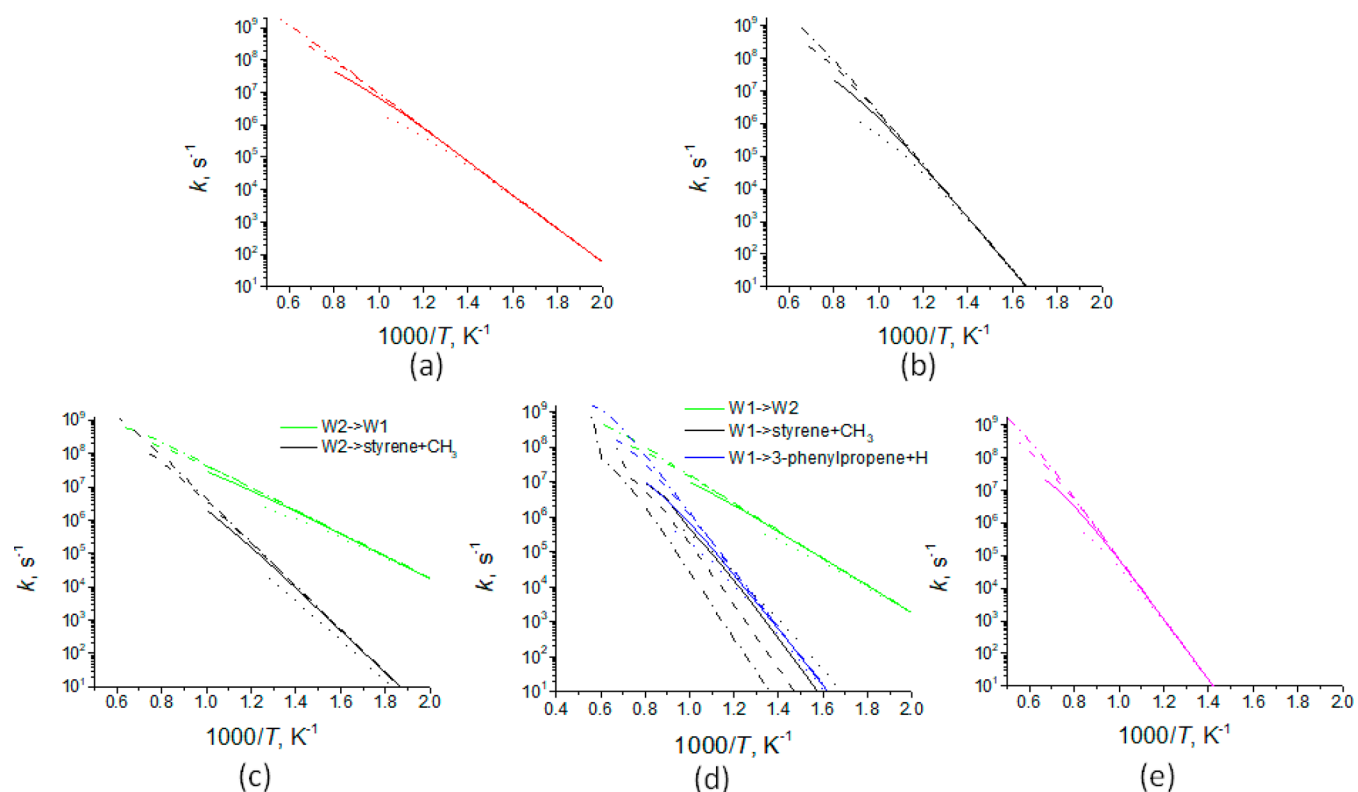


Figure 9. Rate constants for the isomerization and decomposition of various C_9H_{11} isomers: (a) 1-phenyl-prop-3-yl \rightarrow benzyl $C_7H_7 + C_2H_4$; (b) 1-phenyl-prop-1-yl \rightarrow styrene $C_8H_8 + CH_3$; (c) the isomerization of 2-phenyl-prop-3-yl (W2) to 1-phenyl-prop-2-yl (W1) and the dissociation of W2 to styrene + CH_3 ; (d) the isomerization of 1-phenyl-prop-2-yl (W1) to 2-phenyl-prop-3-yl (W2) and the dissociation of W1 to styrene + CH_3 and 3-phenylpropene + H; and (e) 2-phenyl-prop-2-yl \rightarrow 2-phenylpropene + H. The dotted, solid, dashed, and dotted–dashed curves show the values calculated at pressures of 30 Torr and 1, 10, and 100 atm, respectively.

can easily rearrange to 1-phenyl-prop-2-yl W1 by the migration of the phenyl group over the double $C=C$ bond. The calculations show that such an isomerization with the collisional stabilization of W1 is the major fate of W2, except at high pressures and high temperatures when the styrene + CH_3 and 3-phenylpropene + H products are also formed with significant relative yields (Table 5). Hence, in order to reveal the ultimate decomposition products of W2, we need to additionally consider the unimolecular dissociation of W1 (Figure 9d). Again, we can see that the fast isomerization of W1 to the collisionally stabilized intermediate W2 prevails at low temperatures. Above 1000 K, the preferable dissociation pathways of W1 produce styrene + CH_3 and 3-phenylpropene + H with comparable branching ratios, but the latter product is favored by higher temperatures and pressures. At high temperatures, the branching ratio of the C_6H_5 and C_3H_6 bimolecular products of W1 also becomes significant and can

reach 14% (Table 5). The calculated lifetime of 1-phenyl-prop-2-yl W1 with respect to its dissociation to the bimolecular products at 1250 K and 1 atm is 43 ns, nearly the same as for that of 1-phenyl-prop-3-yl. Finally, we consider the decomposition of 2-phenyl-prop-2-yl, which is the main primary product of the pyrolysis of *t*-butylbenzene. This C_9H_{11} isomer nearly exclusively dissociates to 2-phenylpropene by a H-atom loss from one of the methyl groups (Figure 5). The rate constant calculations (Figure 9e) show that 2-phenyl-prop-2-yl can survive up to higher temperatures as compared to the other C_9H_{11} radicals considered above, 1250, 1500, 1800, and 2000 K at 30 Torr and 1, 10, and 100 atm, respectively, and its lifetimes at 1250 and 1500 K at the pressure of 1 atm are 97 and 43 ns, respectively.

Our RRKM-ME calculations also allow us to address the rate constant and product branching ratios of the reaction of benzyl with ethylene (Figure 10a,b). The total rate constant shows

Table 5. Calculated Product Branching Ratios of Various Reactions on the C₉H₁₁ PES

1-Phenyl-prop-3-yl (W4) → Products												
<i>p</i>												
T, K	30 Torr			1 atm			10 atm			100 atm		
	3-phenyl propene	indane	C ₇ H ₇ + C ₂ H ₄	3-phenyl propene	indane	C ₇ H ₇ + C ₂ H ₄	3-phenyl propene	indane	C ₇ H ₇ + C ₂ H ₄	3-phenyl propene	indane	C ₇ H ₇ + C ₂ H ₄
800	0.09%	4.69%	88.76%	0.17%	2.27%	80.69%	0.18%	0.69%	74.41%	0.18%	0.10%	72.23%
900	0.16%	4.80%	95.04%	0.42%	2.61%	88.77%	0.49%	1.17%	83.45%	0.48%	0.25%	80.12%
1000	0.24%	4.28%	95.47%	0.79%	3.34%	95.85%	1.02%	1.50%	88.75%	1.06%	0.45%	85.17%
1125				1.31%	2.87%	95.80%	2.01%	1.66%	91.68%	2.23%	0.71%	88.64%
1250				1.87%	2.56%	95.53%	3.30%	2.22%	94.40%	3.93%	0.89%	89.78%
1375							4.62%	1.97%	93.30%	6.04%	0.97%	89.36%
1500							5.96%	1.80%	92.11%	8.52%	1.59%	89.63%
1650										11.34%	1.41%	86.94%
1800										14.11%	1.27%	84.34%
1-Phenyl-prop-1-yl (W7) → Products												
T, K	30 Torr		1 atm		10 atm		100 atm					
	styrene + CH ₃	trans-1-phenyl propene	styrene + CH ₃	trans-1-phenyl propene	styrene + CH ₃	trans-1-phenyl propene	styrene + CH ₃	trans-1-phenyl propene				
800	98.47%	1.53%	98.12%	1.88%	98.05%	1.94%	98.04%	1.95%				
900	98.15%	1.85%	97.51%	2.48%	97.31%	2.68%	97.26%	2.73%				
1000	97.89%	2.11%	96.97%	3.01%	96.56%	3.42%	96.42%	3.56%				
1125	97.62%	2.37%	96.44%	3.54%	95.72%	4.25%	95.36%	4.60%				
1375			96.01%	3.97%	95.03%	4.93%	94.36%	5.58%				
1500					94.46%	5.49%	93.49%	6.44%				
1650					93.99%	5.95%	92.75%	7.16%				
1800							92.01%	7.89%				
2-Phenyl-prop-3-yl (W2) → Products												
T, K	30 Torr			1 atm			10 atm			100 atm		
	W1	styrene + CH ₃	3-phenyl propene	W1	styrene + CH ₃	3-phenyl propene	W1	styrene + CH ₃	3-phenyl propene	W1	styrene + CH ₃	3-phenyl propene
500	99.99%	0.01%	0.00%	99.99%	0.01%	0.00%	99.99%	0.01%	0.00%	99.99%	0.01%	0.00%
600	99.94%	0.05%	0.00%	99.92%	0.08%	0.00%	99.92%	0.08%	0.00%	99.92%	0.08%	0.00%
700	99.66%	0.27%	0.05%	99.57%	0.40%	0.01%	99.54%	0.43%	0.00%	99.54%	0.44%	0.00%
800	98.36%	1.14%	0.36%	98.47%	1.32%	0.11%	98.35%	1.53%	0.02%	98.33%	1.57%	0.00%
900				95.73%	3.29%	0.59%	95.53%	3.99%	0.14%	95.46%	4.18%	0.02%
1000				90.37%	6.59%	1.98%	90.23%	8.18%	0.63%	90.15%	8.84%	0.10%
1125							79.74%	15.48%	2.30%	79.68%	17.44%	0.48%
1250							66.77%	23.49%	5.03%	66.27%	27.49%	1.44%
1375							54.31%	30.68%	7.90%	52.54%	36.76%	2.94%
1500										40.70%	44.05%	4.51%
1650										29.99%	50.19%	5.96%
1-Phenyl-prop-2-yl (W1) → Products												
T, K	30 Torr				1 atm							
	W2	C ₆ H ₅ + C ₃ H ₆	styrene + CH ₃	3-phenyl propene	W2	C ₆ H ₅ + C ₃ H ₆	styrene + CH ₃	3-phenyl propene				
500	100.00%	0.00%	0.00%	0.00%	100.00%	0.00%	0.00%	0.00%				
600	99.94%	0.00%	0.05%	0.01%	99.98%	0.00%	0.00%	0.01%				
700	99.40%	0.02%	0.42%	0.14%	99.79%	0.02%	0.06%	0.12%				
800	97.10%	0.12%	1.85%	0.78%	98.71%	0.10%	0.43%	0.67%				
900		4.77%	60.57%	28.94%	95.18%	0.42%	1.64%	2.44%				
1000		5.52%	56.83%	31.68%	87.97%	1.14%	3.97%	6.10%				
1125		6.25%	53.42%	34.15%		8.71%	43.21%	41.29%				
1250						9.55%	39.97%	43.55%				
T, K	10 atm				100 atm							
	W2	C ₆ H ₅ + C ₃ H ₆	styrene + CH ₃	3-phenyl propene	W2	C ₆ H ₅ + C ₃ H ₆	styrene + CH ₃	3-phenyl propene				
500	100.00%	0.00%	0.00%	0.00%	100.00%	0.00%	0.00%	0.00%				
600	99.98%	0.00%	0.00%	0.01%	99.98%	0.00%	0.00%	0.01%				
700	99.84%	0.02%	0.01%	0.13%	99.84%	0.02%	0.00%	0.13%				
800	99.05%	0.10%	0.07%	0.71%	99.10%	0.10%	0.01%	0.72%				
900	96.33%	0.44%	0.33%	2.64%	96.54%	0.45%	0.04%	2.72%				
1000	89.80%	1.29%	1.10%	7.09%	90.25%	1.35%	0.15%	7.56%				

Table 5. continued

1-Phenyl-prop-2-yl (W1) → Products												
T, K	30 Torr				1 atm							
	W2	C ₆ H ₅ + C ₃ H ₆	styrene + CH ₃	3-phenyl propene	W2	C ₆ H ₅ + C ₃ H ₆	styrene + CH ₃	3-phenyl propene				
			10 atm				100 atm					
1125	75.81%	3.22%	2.85%	16.43%	75.58%	3.60%	0.52%	18.63%				
1250	59.96%	5.56%	4.65%	27.07%	57.02%	6.59%	1.11%	32.41%				
1375	47.00%	7.63%	5.70%	36.06%	40.92%	9.30%	1.67%	44.22%				
1500		12.25%	31.04%	49.31%	29.70%	11.28%	1.99%	52.47%				
1650					21.38%	12.84%	2.06%	58.72%				
1800						13.96%	31.52%	47.40%				

C ₇ H ₇ + C ₂ H ₄ → Products												
T, K	30 Torr			1 atm			10 atm			100 atm		
	W4	3-phenyl propene	indane	W4	3-phenyl propene	indane	W4	3-phenyl propene	indane	W4	3-phenyl propene	indane
500	99.80%	0.00%	0.03%	99.98%	0.00%	0.00%	100.00%	0.00%	0.00%	100.00%	0.00%	0.00%
600	99.49%	0.00%	0.22%	99.94%	0.00%	0.00%	99.99%	0.00%	0.00%	100.00%	0.00%	0.00%
700	98.79%	0.05%	0.87%	99.84%	0.00%	0.03%	99.97%	0.00%	0.00%	100.00%	0.00%	0.00%
800	97.14%	0.29%	2.33%	99.65%	0.04%	0.14%	99.93%	0.01%	0.01%	99.99%	0.00%	0.00%
900	93.68%	1.34%	4.96%	99.20%	0.22%	0.40%	99.84%	0.03%	0.03%	99.97%	0.00%	0.00%
1000	85.66%	4.96%	9.29%	98.29%	0.86%	0.83%	99.62%	0.16%	0.10%	99.94%	0.02%	0.00%
1125		49.81%	49.37%	94.85%	3.30%	1.78%	98.87%	0.74%	0.26%	99.81%	0.10%	0.02%
1250		67.17%	31.78%	86.79%	9.84%	3.19%	97.00%	2.44%	0.50%	99.46%	0.39%	0.05%
1375		78.48%	20.33%		78.52%	20.28%	92.70%	6.29%	0.89%	98.59%	1.19%	0.11%
1500		85.32%	13.39%		85.34%	13.37%	84.79%	13.59%	1.38%	96.86%	2.89%	0.17%
1650		90.07%	8.57%		90.08%	8.56%		90.13%	8.50%	92.68%	6.85%	0.32%
1800		92.77%	5.81%		92.77%	5.81%		92.80%	5.78%	85.63%	13.59%	0.49%
2000		94.78%	3.74%		94.78%	3.74%		94.79%	3.73%	94.83%	3.68%	3.68%
2250		96.07%	2.38%		96.07%	2.38%		96.07%	2.37%	96.09%	2.35%	2.35%
2500		96.75%	1.64%		96.75%	1.64%		96.75%	1.64%	96.75%	1.63%	1.63%

typical falloff behavior (Figure 10a) in the intermediate temperatures ranges of 700–1125, 800–1375, 1000–1650, and 1250–2000 K at 30 Torr and 1, 10, and 100 atm, respectively. This behavior is attributed to the favorable dissociation of the initial C₉H₁₁ intermediate 1-phenyl-prop-3-yl back to the benzyl and C₂H₄ reactants. Because of this redissociation of the intermediate, the maximal deviations from the HP rate constants reach factors of 20 (1125 K, 30 Torr), 11.7 (1375 K, 1 atm), 6.7 (1650 K, 10 atm), and 4.1 (2000 K, 1000 atm). Above 2000 K, all finite-pressure rate constants merge, and their deviation from the HP values decreases. Such shape of the finite-pressure rate constants is characteristic of a reaction leading to an endothermic bimolecular product via an exothermic intermediate, and it reflects a competition between the collisional stabilization of the intermediate prevailing at low temperatures, its redissociation back to the reactants, and its dissociation to the products, which takes over at high temperatures. It is also noteworthy that, owing to the higher stability of the benzyl radical as compared to that of phenyl, the C₇H₇ + C₂H₄ reaction proceeds via a 37 kJ mol⁻¹ entrance barrier (Figure 1) and is anticipated to be much slower than the C₆H₅ + C₂H₄ reaction. The ratio of the rate constant of the latter and former reactions calculated at 1 atm is as high as 616 at 500 K but decreases to 58.5 and 5.3 at 1500 and 2500 K, respectively. As seen in Figure 10b, at lower temperatures the C₇H₇ + C₂H₄ reaction would mostly produce the collisionally stabilized 1-phenyl-prop-3-yl intermediate, but at higher temperatures, 1000, 1250, 1500, and 1800 K at 30 Torr and 1, 10, and 100 atm, respectively, when this intermediate is no longer stable, 3-phenylpropene and H are predicted to become

the predominant products, with a minor contribution of indane and H.

3.6. Unimolecular Decomposition of C₁₀H₁₃ Radicals. Although C₁₀H₁₃ radicals are not anticipated to be efficiently produced via the unimolecular dissociation of butylbenzene isomers, they can be formed by direct H abstraction, i.e., by H atoms which become available through secondary decomposition of the primary pyrolysis products or by other radicals present in flames. Since the weakest C–H bond in C₁₀H₁₄ is most likely to be attacked in a H-abstraction reaction, here we consider the secondary decomposition for only the most thermodynamically favorable C₁₀H₁₃ products, 1-phenyl-but-1-yl from *n*-butylbenzene, 2-phenyl-but-2-yl from *s*-butylbenzene, and *t*-phenyl-isobutyl from *t*-butylbenzene. The calculated rate constants are illustrated in Figure 11a–c. 1-Phenyl-but-1-yl dissociates by C–C bond β -scission to form styrene and C₂H₅. It should be noted that the H migrations leading to other 1-phenyl-butyl radicals were not considered here because they are not anticipated to compete with β -scission. Only 1,2-, 1,3-, and 1,4-H shifts are feasible in 1-phenyl-but-1-yl, whereas our previous studies of PESs for decyl and dodecyl radicals have shown that only 1,5-, 1,6-, and 1,7-H shifts can be competitive with a C–C bond β -scission process.^{23,24} The RRKM-ME calculations indicate that 1-phenyl-but-1-yl can exist up to temperatures of 1000, 1250, 1375, and 1650 K at pressure of 30 Torr and 1, 10, and 100 atm, respectively, and rapidly equilibrates with the styrene and C₂H₅ products at higher temperatures (Figure 11a). At 1 atm, the calculated lifetime of 1-phenyl-but-1-yl at 1250 K is about 36 ns. Thus, under typical combustion conditions this metastable radical would eliminate

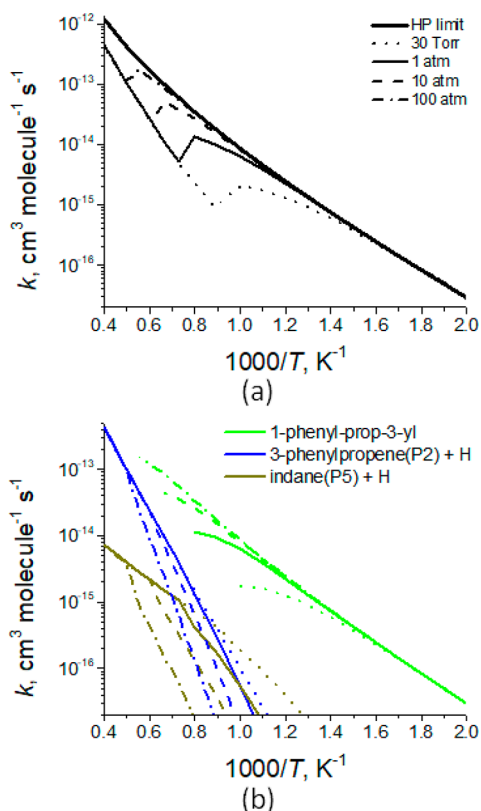


Figure 10. Total (a) and individual channel (b) rate constants for the benzyl $C_7H_7 + C_2H_4$ reaction. The dotted, solid, dashed, and dotted–dashed curves show the values calculated at pressures of 30 Torr and 1, 10, and 100 atm, respectively. The bold curve in panel (a) shows the HP limit total rate constant.

the ethyl radical and form a stable styrene molecule on a nanosecond scale or faster. The 2-phenyl-but-2-yl radical also rapidly decomposes by a C–C bond β -scission producing 2-phenylpropene and CH_3 . The stability of 2-phenyl-but-2-yl is comparable to that of 1-phenyl-but-1-yl, as it is predicted to exist up to the same temperatures at the same pressures, and the lifetime at 1 atm and 1250 K with respect to the decomposition via β -scission is 42 ns (Figure 11b). Finally, *t*-phenyl-isobutyl has two possible distinct C–C bond β -scission pathways leading to 2-phenylpropene + CH_3 and phenyl + isobutyl C_4H_8 (Figure 5). The rate constant calculation shows that the former product channel is dominant (from 99.7 to 97.2% at 30 Torr to 99.7–80.7% at 100 atm), with the latter channel being minor (Figure 11c). The contribution of the phenyl + isobutyl channel grows with temperature, especially at high pressures. *t*-Phenyl-isobutyl appears to be slightly less stable than 1-phenyl-but-1-yl and 2-phenyl-but-2-yl and is predicted to exist up to 900, 1125, 1250, and 1500 K at the four considered pressures, respectively, and its calculated lifetime at the highest temperature studied at 1 atm is only 39 ns. Hence, the fate of *t*-phenyl-isobutyl is to rapidly undergo secondary decomposition predominantly to 2-phenylpropene and CH_3 .

4. CONCLUSIONS

We are now in a position to summarize the nascent pyrolytic products of butylbenzene isomers produced by primary dissociation followed by very fast secondary decomposition. Primary dissociation of *n*-butylbenzene produces mostly benzyl radical $C_7H_7 + C_3H_7$ and C_8H_9 ($C_6H_5C_2H_4$) + C_2H_5 with

relative yields varying with temperature and pressure and a minor amount of 1-phenyl-prop-3-yl + CH_3 . Fast secondary decomposition reactions break C_3H_7 into $C_2H_4 + CH_3$, C_2H_5 into $C_2H_4 + H$, $C_6H_5C_2H_4$ mostly into styrene + H and to a lesser extent $C_6H_5 + C_2H_4$, and 1-phenyl-prop-3-yl mostly into benzyl + C_2H_4 . Under the conditions where H atoms or other reactive radicals are available, the 1-phenyl-but-1-yl radical can also be formed as a primary product, which then rapidly dissociates to styrene + C_2H_5 and further to styrene + $C_2H_4 + H$. On the basis of this consideration, the main fragments of the pyrolysis of *n*-butylbenzene should include (in the order of decreasing mass) styrene C_8H_8 , benzyl C_7H_7 , ethylene C_2H_4 , methyl CH_3 , and H atoms. This conclusion concurs with the results of the recent experimental study of the *n*-butylbenzene pyrolysis in a flow reactor using synchrotron vacuum ultraviolet photoionization mass spectrometry for the product detection,⁴³ which showed styrene, benzyl, and ethylene to be formed in the highest mole fractions, along with ethylbenzene, toluene, methane, and ethane, whereas the yield of CH_3 was relatively low. According to our calculations, ethylbenzene, toluene, methane, and ethane are not nascent products. These stable molecules are probably produced via the recombination of benzyl with CH_3 , benzyl with H, CH_3 with H, and CH_3 with CH_3 or C_2H_5 with H. Such recombination processes would also clearly reduce the observed yield of methyl radicals. Another noticeable observed product, benzene, can be formed via the $C_6H_5 + H$ reaction. On the basis of their modeling results, the authors of this experimental work deduced⁴³ that the benzylic C–C bond dissociation leading to C_7H_7 and C_3H_7 was the key decomposition reaction of *n*-butylbenzene under all considered conditions and H abstraction gave increasing contributions with rising pressure. Indeed, the observed mole fraction of styrene grows with temperature and pressure, which can be due to two factors: an increasing primary yield of the $C_6H_5C_2H_4$ radical further decomposing to styrene + H and the contribution of the H abstraction reaction forming 1-phenyl-but-1-yl and rapidly dissociating to styrene + C_2H_5 . The kinetic modeling results showed reasonable qualitative agreement with the experimental mole fractions, but we expect that the use of the physics-based rate constants generated here from high-level quantum chemical and RRKM-ME calculations can improve the accuracy and reliability of the models and lend them predictive power.

Li, Dagaut, and co-workers have recently published a series of works describing experimental and kinetic modeling studies for a series of alkylbenzenes including toluene,^{83,84} ethylbenzene,⁸⁵ and *n*-propylbenzene.⁸⁶ Direct comparison is not warranted because the experiments in a jet-stirred reactor occur on a longer time scale and the kinetic modeling takes into account thousands of secondary reactions following the primary pyrolysis process, whereas our calculations consider the nascent pyrolytic products formed in the unimolecular primary and fast secondary decompositions. Nevertheless, our present results are in accord with the conclusions of Li, Dagaut, and co-workers that the benzyl radical and styrene are the critical intermediates in the pyrolysis and oxidation of alkylbenzenes (with exception that for toluene styrene is not important) and that the benzylic C–C bond dissociation reaction is the dominant decomposition channel (benzylic C–H bond for toluene). As the alkyl side chain elongates, the additional alkylic C–C bond cleavages also contribute, as do H-abstraction pathways under certain conditions. Li, Dagaut, and co-workers have shown that benzyl and styrene participate in the consequent growth of PAHs, such as naphthalene and indene; hence, similar PAH growth

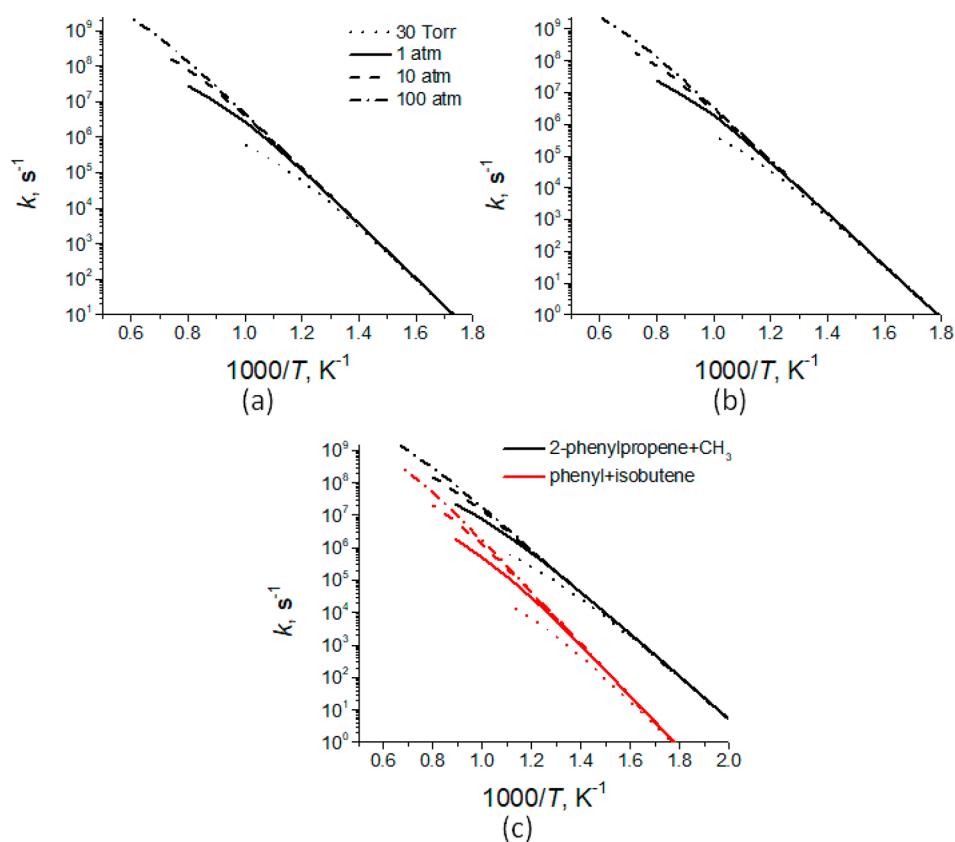


Figure 11. Rate constants for the unimolecular decomposition of various $C_{10}H_{13}$ radicals: (a) 1-phenyl-but-1-yl, (b) 2-phenyl-but-2-yl, and (c) *t*-phenyl-isobutyl. The dotted, solid, dashed, and dotted–dashed curves show the values calculated at pressures of 30 Torr and 1, 10, and 100 atm, respectively.

processes can be significant at later stages of the butylbenzene pyrolysis.

The primary decomposition of *s*-butylbenzene is expected to form C_8H_9 ($C_6H_5CHCH_3$) + C_2H_5 and a minor amount of C_9H_{11} (1-phenyl-prop-1-yl) + CH_3 . $C_6H_5CHCH_3$ undergoes secondary decomposition predominantly to styrene + H, whereas 1-phenyl-prop-1-yl rapidly dissociates to styrene + CH_3 . If the 2-phenyl-but-2-yl radical can be formed by direct H abstraction then its dominant secondary dissociation channel produces 2-phenylpropene C_9H_{10} + CH_3 . Thus, we anticipate that the main nascent pyrolysis products of *s*-butylbenzene should include styrene, ethylene (from C_2H_5), CH_3 , H, and 2-phenylpropene, where the relative yield of the latter would correlate with the feasibility of direct H abstraction from the parent molecule. The largest difference in the pyrolysis of *s*-butylbenzene from that of *n*-butylbenzene is the absence of the nascent benzyl radical product, which can be traced to the molecular structure; *s*-butylbenzene does not have a $C_6H_5CH_2$ fragment. As in *n*-butylbenzene, the two benzylic C–C bonds in *s*-butylbenzene are the weakest, and their cleavage dominates the primary decomposition process.

Finally, *t*-butylbenzene gives 2-phenyl-prop-2-yl + CH_3 as a nearly exclusive primary product through the cleavage of one of the three equivalent C–C benzylic bonds. This is in agreement with the experimental results by Troe et al., who observed the formation of 2-phenyl-prop-2-yl and methyl radicals using flash photolysis followed by UV–vis spectroscopy.³⁹ However, our results do not support the suggestion by Ma et al.⁴⁰ concerning the initial formation of phenyl C_6H_5 and *t*- C_4H_9 . Furthermore, 2-phenyl-prop-2-yl rapidly and also nearly exclusively forms 2-

phenylpropene + H. Considering the possibility of a direct H abstraction from a methyl group, *t*-phenyl-isobutyl $C_{10}H_{13}$ can be formed and then undergoes fast secondary decomposition mostly to 2-phenylpropene + CH_3 and a minor amount of phenyl + isobutene, increasing with temperature and pressure. Thus, 2-phenylpropene, CH_3 , and H are anticipated to be the dominant nascent products of the pyrolysis of *t*-butylbenzene, whereas phenyl and isobutene could be minor products serving as tracers of the contribution of H abstraction from the parent molecule. Clearly, the product menagerie from *t*-butylbenzene pyrolysis is expected to be much narrower than for the other butylbenzene isomers. The most striking difference is the absence of ethylene, which is the main pyrolysis product of alkanes and also makes a large contribution in the decomposition of *n*- and *s*-butylbenzenes. Again, this difference can be attributed to the molecular structure of *t*-butylbenzene, which does not feature any CH_2 groups.

In summary, the three butylbenzene isomers considered produce rather different nascent pyrolysis fragments, although there is a significant overlap between *n*- and *s*-butylbenzene. The presence of different fragments in distinguishable amounts can therefore influence the oxidation mechanism of these fuel components and hence affect the kinetics of their combustion. Pressure- and temperature-dependent rate constants generated here in the initial stages of pyrolysis of butylbenzenes assembled in Table 2 are recommended for kinetic modeling.

■ AUTHOR INFORMATION

Corresponding Authors

*E-mail: mebela@fiu.edu.

*E-mail: ralfk@hawaii.edu.

ORCID 

Alexander M. Mebel: 0000-0002-7233-3133

Notes

The authors declare no competing financial interest.

ACKNOWLEDGMENTS

This project is supported by the Air Force Office of Scientific Research (AFOSR) under grant no. FA9550-15-1-0011 to the University of Hawaii and Florida International University.

REFERENCES

- (1) Bruno, T. J.; Abel, K. R.; Riggs, J. R. Comparison of JP-8 and JP-8 + 100 with the Advanced Distillation Curve Approach. *Energy Fuels* **2012**, *26*, 5843–5850.
- (2) Bezaire, N.; Wadumesthrige, K.; Simon, Ng K. Y.; Salley, S. O. Limitations of the Use of Cetane Index for Alternative Compression Ignition Engine Fuels. *Fuel* **2010**, *89*, 3807–3813.
- (3) Gregg, S. D.; Campbell, J. L.; Fisher, J. W.; Bartlett, M. G. Methods for the Characterization of Jet Propellant-8: Vapor and Aerosol. *Biomed. Chromatogr.* **2007**, *21*, 463–472.
- (4) Gough, R. V.; Bruno, T. J. Composition-Explicit Distillation Curves of Alternative Turbine Fuels. *Energy Fuels* **2013**, *27*, 294–302.
- (5) Meylemans, H. A.; Baldwin, L. C.; Harvey, B. G. Low-Temperature Properties of Renewable High-Density Fuel Blends. *Energy Fuels* **2013**, *27*, 883–888.
- (6) Witten, M. L.; Zeiger, E.; Ritchie, G. D. *Jet Fuel Toxicology*; CRC Press: Boca Raton, FL, 2011.
- (7) Rodgers, R. P.; Blumer, E. N.; Freitas, M. A.; Marshall, A. G. Jet Fuel Chemical Composition, Weathering, and Identification as a Contaminant at a Remediation Site, Determined by Fourier Transform Ion Cyclotron Resonance Mass Spectrometry. *Anal. Chem.* **1999**, *71*, S171–S176.
- (8) DuBois, T. G.; Nieh, S. *Effects of Hydrocarbon Chemical Class Composition on Autothermal Reforming of JP-8 Fuel*; Curran Associates, Inc.: Las Vegas, 2010.
- (9) Echavarria, C. A.; Jaramillo, I. C.; Sarofim, A. F.; Lighty, J. S. Burnout of Soot Particles in a Two-Stage Burner with a JP-8 Surrogate Fuel. *Combust. Flame* **2012**, *159*, 2441–2448.
- (10) Wang, H.; Oehlschlaeger, M. A. Autoignition Studies of Conventional and Fischer–Tropsch Jet Fuels. *Fuel* **2012**, *98*, 249–258.
- (11) Merrill, E. A.; Gearhart, J. M.; Sterner, T. R.; Robinson, P. J. Improved Predictive Model for n-Decane Kinetics across Species, as a Component of Hydrocarbon Mixtures. *Inhalation Toxicol.* **2008**, *20*, 851–863.
- (12) Troe, J. Toward a Quantitative Understanding of Elementary Combustion Reactions. *Symp. Combust., [Proc.]* **1989**, *22*, 843–862.
- (13) Cox, R. A. *Kinetics and Mechanisms of Elementary Chemical Processes of Importance in Combustion. CEC Contract Final Report, EUR 12772*. Harwell Lab: Harwell, U.K., 1990.
- (14) Baulch, D. L.; Cobos, C. J.; Cox, R. A.; Esser, C.; Frank, P.; Just, Th.; Kerr, J. A.; Pilling, M. J.; Troe, J.; Walker, R. W.; et al. Evaluated Kinetic Data for Combustion Modeling. *J. Phys. Chem. Ref. Data* **1992**, *21*, 411–734.
- (15) Baulch, D. L.; Bowman, C. T.; Cobos, C. J.; Cox, R. A.; Just, Th.; Kerr, J. A.; Pilling, M. J.; Stocker, D.; Troe, J.; Tsang, W.; et al. Evaluated Kinetic Data for Combustion Modeling: Supplement II. *J. Phys. Chem. Ref. Data* **2005**, *34*, 757–1397.
- (16) Miller, J. A.; Pilling, M. J.; Troe, J. Unravelling Combustion Mechanisms through a Quantitative Understanding of Elementary Reactions. *Proc. Combust. Inst.* **2005**, *30*, 43–88.
- (17) Sun, C.; Sung, C. J.; Wang, H.; Law, C. K. On the Structure of Nonsooting Counterflow Ethylene and Acetylene Diffusion Flames. *Combust. Flame* **1996**, *107*, 321–335.
- (18) Banerjee, S.; Tangko, R.; Sheen, D. A.; Wang, H.; Bowman, C. T. An Experimental and Kinetic Modeling Study of n-Dodecane Pyrolysis and Oxidation. *Combust. Flame* **2016**, *163*, 12–30.
- (19) Smolke, J.; Carbone, F.; Egolfopoulos, F. N.; Wang, H. Effect of n-Dodecane Decomposition on its Fundamental Flame Properties. *Combust. Flame* **2018**, *190*, 65–73.
- (20) Violi, A.; Yan, S.; Eddings, E. G.; Sarofim, F.; Granata, S.; Faravelli, T.; Ranzi, E. Experimental Formulation and Kinetic Model for JP-8 Surrogate Mixtures. *Combust. Sci. Technol.* **2002**, *174*, 399–417.
- (21) Mawid, M. A.; Park, T. W.; Sekar, B.; Arana, C. *Development and Validation of A Detailed JP-8 Fuel Chemistry Model*, 2nd JANNAF Modeling and Simulation Subcommittee Meeting, Destin, FL, 2002.
- (22) Podlesak, T.; Hendrickson, M.; Matthews, S.; Nawrocki, E.; Seibert, M.; Zalewski, M. Army Stirling Engine Research and Development - Past, Present and Future. *Proc. Power Sources Conference* **2010**, *44*, 462–465.
- (23) Zhao, L.; Yang, T.; Kaiser, R. I.; Troy, T. P.; Ahmed, M.; Belisario-Lara, D.; Ribeiro, J. M.; Mebel, A. M. Combined Experimental and Computational Study on the Unimolecular Decomposition of JP-8 Jet Fuel Surrogates. I. n-Decane (n-C₁₀H₂₂). *J. Phys. Chem. A* **2017**, *121*, 1261–1280.
- (24) Zhao, L.; Yang, T.; Kaiser, R. I.; Troy, T. P.; Ahmed, M.; Ribeiro, J. M.; Belisario-Lara, D.; Mebel, A. M. Combined Experimental and Computational Study on the Unimolecular Decomposition of JP-8 Jet Fuel Surrogates. II: n-Dodecane (n-C₁₂H₂₆). *J. Phys. Chem. A* **2017**, *121*, 1281–1297.
- (25) Zhang, F.; Kaiser, R. I.; Kislov, V. V.; Mebel, A. M.; Golan, A.; Ahmed, M. A VUV Photoionization Study of the Formation of the Indene Molecule and Its Isomers. *J. Phys. Chem. Lett.* **2011**, *2*, 1731–1735.
- (26) Zhang, F.; Kaiser, R. I.; Golan, A.; Ahmed, M.; Hansen, N. A VUV Photoionization Study of the Combustion-Relevant Reaction of the Phenyl Radical (C₆H₅) with Propylene (C₃H₆) in a High Temperature Chemical Reactors. *J. Phys. Chem. A* **2012**, *116*, 3541–3546.
- (27) Kaiser, R. I.; Belau, L.; Leone, S. R.; Ahmed, M.; Wang, Y. M.; Braams, B. J.; Bowman, J. M. A Combined Experimental and Computational Study on the Ionization Energies of the Cyclic and Linear C₃H Isomers. *ChemPhysChem* **2007**, *8*, 1236–1239.
- (28) Kaiser, R. I.; Mebel, A.; Kostko, O.; Ahmed, M. On the Ionization Potentials of C₄H₃ Isomers. *Chem. Phys. Lett.* **2010**, *485*, 281–285.
- (29) Kaiser, R. I.; Sun, B. J.; Lin, H. M.; Chang, A. H. H.; Mebel, A. M.; Kostko, O.; Ahmed, M. An Experimental and Theoretical Study on the Ionization Energies of Polyynes (H(CC)_nH; n = 1–9). *Astrophys. J.* **2010**, *719*, 1884–1889.
- (30) Kaiser, R. I.; Maksyutenko, P.; Ennis, C.; Zhang, F. T.; Gu, X. B.; Krishtal, S. P.; Mebel, A. M.; Kostko, O.; Ahmed, M. Untangling the Chemical Evolution of Titan's Atmosphere and Surface - From Homogeneous to Heterogeneous Chemistry. *Faraday Discuss.* **2010**, *147*, 429–478.
- (31) Kaiser, R. I.; Krishtal, S. P.; Mebel, A. M.; Kostko, O.; Ahmed, M. An Experimental and Theoretical Study of the Ionization Energies of SiC₂H_x (x = 0, 1, 2) Isomers. *Astrophys. J.* **2012**, *761*, 178–178.
- (32) Golan, A.; Ahmed, M.; Mebel, A. M.; Kaiser, R. I. A VUV Photoionization Study on the Multichannel Reaction of Phenyl Radicals with 1,3-butadiene Under Combustion Relevant Conditions. *Phys. Chem. Chem. Phys.* **2013**, *15*, 341–347.
- (33) Kostko, O.; Zhou, J.; Sun, B. J.; Shiuang Lie, J.; Chang, A. H. H.; Kaiser, R. I.; Ahmed, M. Determination of Ionization Energies of C_nN (n = 4–12): Vacuum Ultraviolet Photoionization Experiments and Theoretical Calculations. *Astrophys. J.* **2010**, *717*, 674–682.
- (34) Parker, D. S.; Kaiser, R. I.; Troy, T. P.; Ahmed, M. Hydrogen Abstraction/Acetylene Addition Revealed. *Angew. Chem., Int. Ed.* **2014**, *53*, 7740–7744.
- (35) Yahagi, N. Pyrolysis of tert-Butylbenzene in the Presence of Hydrogen. *Sekiyu Gakkaishi* **1981**, *24*, 1–8.

- (36) Badger, G. M.; Spotswood, T. M. Formation of Aromatic Hydrocarbons at High Temperatures. IX. Pyrolysis of Toluene, Ethylbenzene, Propylbenzene, and Butylbenzene. *J. Chem. Soc.* **1960**, 4420–4427.
- (37) Leigh, C. H.; Szwarc, M. The Pyrolysis of Butylbenzene and the Heat of Formation of Propyl Radical. *J. Chem. Phys.* **1952**, *20*, 407–411.
- (38) Tsang, W. Hydrocarbon Decomposition. 6. Thermal Decomposition of 3,4-Dimethylhexane, 2,2,3-Trimethylpentane, tert-Butylcyclohexane, and Related Hydrocarbons. *J. Phys. Chem.* **1972**, *76*, 143–156.
- (39) Brand, U.; Hippler, H.; Lindemann, L.; Troe, J. C-C and C-H Bond Splits of Laser-Excited Aromatic-Molecules. 1. Specific and Thermally Averaged Rate Constants. *J. Phys. Chem.* **1990**, *94*, 6305–6316.
- (40) Ma, X.; Peng, Y.; Schobert, H. H. Effects of Structure of the Butyl Chain on the Pyrolysis of Butylbenzenes: Molecular Simulation and Mechanism. *Prepr. - Am. Chem. Soc., Div. Pet. Chem.* **2000**, *45*, 488–492.
- (41) Peng, Y.; Schobert, H. H.; Song, C.; Hatcher, P. G. Thermal Decomposition Studies of Jet Fuel Components: n-Butylbenzene and t-Butylbenzene. *Prepr. - Am. Chem. Soc., Div. Pet. Chem.* **1992**, *37*, 505–513.
- (42) Freund, H.; Olmstead, W. N. Detailed Chemical Kinetic Modeling of Butylbenzene Pyrolysis. *Int. J. Chem. Kinet.* **1989**, *21*, 561–574.
- (43) Zhang, Y.; Cao, C.; Li, Y.; Yuan, W.; Yang, X.; Yang, J.; Qi, F.; Huang, T.-P.; Lee, Y.-Y. Pyrolysis of n-Butylbenzene at Various Pressures: Influence of Long Side-Chain Structure on Alkylbenzene Pyrolysis. *Energy Fuels* **2017**, *31*, 14270–14279.
- (44) Tong, X.; Ford, M. S.; Dessent, C. E. H.; Muller-Dethlefs, K. The Effect of Conformation on the Ionization Energetics of n-Butylbenzene. I. A Threshold Ionization Study. *J. Chem. Phys.* **2003**, *119*, 12908–12913.
- (45) Tong, X.; Cerny, J.; Muller-Dethlefs, K.; Dessent, C. E. H. Effect of Noncovalent Interactions on Conformers of The n-Butylbenzene Monomer Studied by Mass Analyzed Threshold Ionization Spectroscopy and Basis-Set Convergent Ab Initio Computations. *J. Phys. Chem. A* **2008**, *112*, 5866–5871.
- (46) Mate, B.; Suenram, R. D.; Lugez, C. Microwave Studies of Three Alkylbenzenes: Ethyl, n-propyl, and n-Butylbenzene. *J. Chem. Phys.* **2000**, *113*, 192–199.
- (47) Campanelli, A. R.; Ramondo, F.; Domenicano, A.; Hargittai, I. Molecular-Structure and Conformation of Tert-Butylbenzene - a Concerted Study by Gas-Phase Electron-Diffraction and Theoretical Calculations. *J. Phys. Chem.* **1994**, *98*, 11046–11052.
- (48) Halbert, S.; Clavaguera, C.; Bouchoux, G. The Shape of Gaseous n-Butylbenzene: Assessment of Computational Methods and Comparison with Experiments. *J. Comput. Chem.* **2011**, *32*, 1550–1560.
- (49) Mo, O.; Yanez, M.; Elguero, J.; Roux, M. V.; Jimenez, P.; Davalos, J. Z.; da Silva, M. A. V.; da Silva, M. D. D. M. C.; Cabildo, P.; Claramunt, R. Substituent Effects on Enthalpies of Formation: Benzene Derivatives. *J. Phys. Chem. A* **2003**, *107*, 366–371.
- (50) Van Speybroeck, V.; Borremans, Y.; Van Neck, D.; Waroquier, M.; Wauters, S.; Saeys, M.; Marin, G. B. Ab Initio Study of Radical Reactions: Cyclization Pathways for the Butylbenzene Radical (II). *J. Phys. Chem. A* **2001**, *105*, 7713–7723.
- (51) Becke, A. D. Density-Functional Thermochemistry. III. The Role of Exact Exchange. *J. Chem. Phys.* **1993**, *98*, 5648–5652.
- (52) Lee, C.; Yang, W.; Parr, R. G. Development of the Colle-Salvetti Correlation-Energy Formula into a Functional of the Electron Density. *Phys. Rev. B: Condens. Matter Mater. Phys.* **1988**, *37*, 785–789.
- (53) Curtiss, L. A.; Raghavachari, K.; Redfern, P. C.; Rassolov, V.; Pople, J. A. Gaussian-3 (G3) Theory for Molecules Containing First and Second-Row Atoms. *J. Chem. Phys.* **1998**, *109*, 7764–7776.
- (54) Curtiss, L. A.; Raghavachari, K.; Redfern, P. C.; Baboul, A. G.; Pople, J. A. Gaussian-3 Theory Using Coupled Cluster Energies. *Chem. Phys. Lett.* **1999**, *314*, 101–107.
- (55) Baboul, A. G.; Curtiss, L. A.; Redfern, P. C.; Raghavachari, K. Gaussian-3 Theory Using Density Functional Geometries and ZeroPoint Energies. *J. Chem. Phys.* **1999**, *110*, 7650–7657.
- (56) Kislov, V. V.; Mebel, A. M.; Aguilera-Iparraguirre, J.; Green, W. H. The Reaction of Phenyl Radical with Propylene as a Possible Source of Indene and Other Polycyclic Aromatic Hydrocarbons: An Ab Initio/RRKM-ME Study. *J. Phys. Chem. A* **2012**, *116*, 4176–4191.
- (57) Grimme, S. Semiempirical Hybrid Density Functional with Perturbative Second-Order Correlation. *J. Chem. Phys.* **2006**, *124*, 034108.
- (58) Goerigk, L.; Grimme, S. Efficient and Accurate Double-Hybrid-Meta-GGA Density Functionals—Evaluation with the Extended GMTKN30 Database for General Main Group Thermochemistry, Kinetics, and Noncovalent Interactions. *J. Chem. Theory Comput.* **2011**, *7*, 291–309.
- (59) Grimme, S.; Ehrlich, S.; Goerigk, L. Effect of the Damping Function in Dispersion Corrected Density Functional Theory. *J. Comput. Chem.* **2011**, *32*, 1456–1465.
- (60) Dunning, T. H. Gaussian Basis Sets for Use in Correlated Molecular Calculations. I. The Atoms Boron through Neon and Hydrogen. *J. Chem. Phys.* **1989**, *90*, 1007–1023.
- (61) Adler, T. B.; Knizia, G.; Werner, H.-J. A Simple and Efficient CCSD(T)-F12 Approximation. *J. Chem. Phys.* **2007**, *127*, 221106.
- (62) Knizia, G.; Adler, T. B.; Werner, H.-J. Simplified CCSD(T)-F12 Methods: Theory and Benchmarks. *J. Chem. Phys.* **2009**, *130*, 054104.
- (63) Frisch, M. J.; Trucks, G. W.; Schlegel, H. B.; Scuseria, G. E.; Robb, M. A.; Cheeseman, J. R.; Scalmani, G.; Barone, V.; Mennucci, B.; Petersson, G. A., et al. *Gaussian 09*, Revision A.1; Gaussian, Inc.: Wallingford, CT, 2009.
- (64) Werner, H.-J.; Knowles, P. J.; Knizia, G.; Manby, F. R.; Schütz, M.; Celani, P.; Gyröffy, W.; Kats, D.; Korona, T.; Lindh, R., et al. *MOLPRO*, version 2010.1, a package of ab initio programs, see <http://www.molpro.net>.
- (65) Georgievskii, Y.; Miller, J. A.; Burke, M. P.; Klippenstein, S. J. Reformulation and Solution of the Master Equation for Multiple-Well Chemical Reactions. *J. Phys. Chem. A* **2013**, *117*, 12146–12154.
- (66) Georgievskii, Y.; Klippenstein, S. J. 2015, available online at <http://tcg.cse.anl.gov/papr/codes/mess.html>.
- (67) Mebel, A. M.; Georgievskii, Y.; Jasper, A. W.; Klippenstein, S. J. Pressure-Dependent Rate Constants for PAH Growth: Formation of Indene and its Conversion to Naphthalene. *Faraday Discuss.* **2016**, *195*, 637–670.
- (68) Zheng, J.; Yu, T.; Papajak, E.; Alecu, I. M.; Mielke, S. L.; Truhlar, D. G. Practical Methods for Including Torsional Anharmonicity in Thermochemical Calculations on Complex Molecules: The Internal-Coordinate Multi-Structural Approximation. *Phys. Chem. Chem. Phys.* **2011**, *13*, 10885–10907.
- (69) Troe, J. Theory of Thermal Unimolecular Reactions at Low-Pressures. I. Solutions of Master Equation. *J. Chem. Phys.* **1977**, *66*, 4745–4757.
- (70) Jasper, A. W.; Oana, C. M.; Miller, J. A. Third-Body Collision Efficiencies from Combustion Modeling: Hydrocarbons in Atomic and Diatomic Baths. *Proc. Combust. Inst.* **2015**, *35*, 197–204.
- (71) Jasper, A. W.; Miller, J. A. Lennard-Jones Parameters for Combustion and Chemical Kinetics Modeling from Full-Dimensional Intermolecular Potentials. *Combust. Flame* **2014**, *161*, 101–110.
- (72) Mebel, A. M.; Georgievskii, Y.; Jasper, A. W.; Klippenstein, S. J. Temperature- and Pressure-Dependent Rate Coefficients for the HACA Pathways from Benzene to Naphthalene. *Proc. Combust. Inst.* **2017**, *36*, 919–926.
- (73) Miller, J. A.; Klippenstein, S. J. Determining Phenomenological Rate Coefficients from a Time-Dependent, Multiple-Well Master Equation: “Species Reduction” at High Temperatures. *Phys. Chem. Chem. Phys.* **2013**, *15*, 4744–4753.
- (74) Klippenstein, S. J.; Cline, J. I. Classical Phase Space Theory for Product State Distributions with Application to the V-J Vector Correlation. *J. Chem. Phys.* **1995**, *103*, 5451–5460.

(75) Klippenstein, S. J.; Georgievskii, Y.; Harding, L. B. Predictive Theory for the Combination Kinetics of Two Alkyl Radicals. *Phys. Chem. Chem. Phys.* **2006**, *8*, 1133–1147.

(76) Harding, L. B.; Georgievskii, Y.; Klippenstein, S. J. Predictive Theory for Hydrogen Atom-Hydrocarbon Radical Association Kinetics. *J. Phys. Chem. A* **2005**, *109*, 4646–4656.

(77) Harding, L. B.; Klippenstein, S. J.; Georgievskii, Y. On the Combination Reactions of Hydrogen Atoms with Resonance-Stabilized Hydrocarbon Radicals. *J. Phys. Chem. A* **2007**, *111*, 3789–3801.

(78) Ruscic, B. Active Thermochemical Tables, available at <http://atct.anl.gov>.

(79) Tokmakov, I. V.; Lin, M. C. Combined Quantum Chemical/RRKM-ME Computational Study of the Phenyl + Ethylene, Vinyl + Benzene, and H + Styrene Reactions. *J. Phys. Chem. A* **2004**, *108*, 9697–9714.

(80) Yu, T.; Lin, M. C. Kinetics of the Phenyl Radical Reaction with Ethylene: An RRKM Theoretical Analysis of Low and High Temperature Data. *Combust. Flame* **1995**, *100*, 169–176.

(81) Fahr, A.; Mallard, W. G.; Stein, S. E. Reactions of Phenyl Radicals with Ethene, Ethyne, and Benzene. *Symp. (Int.) Combust., [Proc.]* **1988**, *21*, 825–831.

(82) Fahr, A.; Stein, S. E. Reactions of Vinyl and Phenyl Radicals with Ethyne, Ethene and Benzene. *Symp. (Int.) Combust., [Proc.]* **1989**, *22*, 1023–1029.

(83) Yuan, W.; Li, Y.; Dagaut, P.; Yang, J.; Qi, F. Investigation on the Pyrolysis and Oxidation of Toluene over a Wide Range Conditions. I. Flow Reactor Pyrolysis and Jet Stirred Reactor Oxidation. *Combust. Flame* **2015**, *162*, 3–21.

(84) Yuan, W.; Li, Y.; Dagaut, P.; Yang, J.; Qi, F. Investigation on the Pyrolysis and Oxidation of Toluene over a Wide Range Conditions. II. A Comprehensive Kinetic Modeling Study. *Combust. Flame* **2015**, *162*, 22–40.

(85) Yuan, W.; Li, Y.; Pengloan, G.; Togbe, C.; Dagaut, P.; Qi, F. A Comprehensive Experimental and Kinetic Modeling Study of Ethylbenzene Combustion. *Combust. Flame* **2016**, *166*, 255–265.

(86) Yuan, W.; Li, Y.; Dagaut, P.; Wang, Y.; Wang, Z.; Qi, F. A Comprehensive Experimental and Kinetic Modeling Study of *n*-Propylbenzene Combustion. *Combust. Flame* **2017**, *186*, 178–192.